ELSEVIER

Contents lists available at ScienceDirect

# **Materials Today Communications**

journal homepage: www.elsevier.com/locate/mtcomm





# A review of aging, degradation, and reusability of PA12 powders in selective laser sintering additive manufacturing

Feifei Yang <sup>a</sup>, Navid Zobeiry <sup>b</sup>, Ramulu Mamidala <sup>a</sup>, Xu Chen <sup>a,\*</sup>

- <sup>a</sup> Department of Mechanical Engineering, University of Washington, Seattle, WA 98195, USA
- <sup>b</sup> Department of Materials Science and Engineering, University of Washington, Seattle, WA 98195, USA

# ARTICLE INFO

# Keywords: Polyamide 12 powder Degradation behavior Selective laser sintering (SLS) Aging mechanism Parameter setting

#### ABSTRACT

A popular form of additive manufacturing, selective laser sintering (SLS) enables the unprecedented making of complex 3D parts with high mechanical performance. The semi-crystalline polymer polyamide 12 (PA12) has been extensively used in SLS thanks to its superior mechanical properties, broad sintering window, ease of processibility, reduced warpage and porosity. However, low utilization of the costly feedstock hinders the long-term sustainability of SLS in the industry. Reprocessing and reusing the un-sintered materials with quality assurance have thus appeared as an important and time-sensitive problem. Yet, the feedstocks undergo complex thermal and chemical degradations in SLS. Little results exist to uncover fully the sophisticated process and the reusability of PA12 powders. This review aims to present the state-of-the-art on important aspects of aging mechanisms and degradation behaviors of PA12 powders in SLS. We review first the mechanism of PA12 aging at the molecular scale. Then for the properties of the aged powders, we analyze the evolution of microstructures and geometric properties. Besides, for 3D-printed parts with recycled powders, we cover changes of mechanical properties from tensile strength to Young's modulus. Finally, we provide guidelines and principles of parameter settings when using reclaimed PA12 powders.

# 1. Introduction

Extensively studied and applied to making complex products ranging from micro- to macro-scales directly from a digital model, additive manufacturing is poised to become an underpinning of the next industrial revolution [1–4]. A powder-based additive manufacturing process capable of fabricating complex metallic and high-performance polymeric parts [5,6], selective laser sintering (SLS) represents one popular and high-end 3D printing technique [7–9]. Among the suitable materials for SLS, polymers were the first and one of the most applied [10], owing to the low processing temperature, low laser power, and high dimensional accuracy of the printed parts [11]. In particular, polyamide 12 (PA12) is the most commonly applied semi-crystallize polymer for SLS in medical, automotive, aerospace, and biomedical industries [1,12,13].

Despite the significant capabilities and continuously evolving potentials of SLS, low utilization of raw materials challenges industrial production [14–16]. In a typical build,  $80\sim90\%$  of the expensive (e.g., \$150/kg [17]} powder material remains unmolten in the build chamber [18–21]. Not only is the low utilization of materials wasteful, collecting and disposing of the powders are also labor-intensive, and

environmentally burdensome. Therefore, reprocessing and reusing the unmolten materials in SLS is of great significance and necessity for broader and more sustainable adoption of the technology [22].

At the core of reusing polymers is to control the degradation behavior of the materials. Prior works of Chen et al. [18] and Dadbakhsh et al. [19] investigated how powders deteriorate and the resulting impact on the evolution of part microstructures. Wudy et al. [23] identified the aging effects of PA12 on molecular weight distribution and thermal properties. Dotchev et al. [20], Wegner et al. [24], and Josupeit et al. [25] showed that the melt volume flow rate (MVR) can work as an effective index of powder flowability powder-degradation rate (when the other parameters remain unchanged). Feng et al. [12] and Chen et al. [26] studied the processability and recyclability of reclaimed PA12 powders into new functional parts. Goodridge et al. [27], Wudy et al. [28], Kozlovsky et al. [29], and Yao et al. [30] identified the influences of powder degradation on mechanical properties of the 3D printed parts. Literature also studied the relationships between process parameter settings and part properties when applying aged powders. Commonly tested parameters include the pre-heating temperature, inter-layer time, and energy density [24,

E-mail addresses: yangff@uw.edu (F. Yang), navidz@uw.edu (N. Zobeiry), ramulum@uw.edu (R. Mamidala), chx@uw.edu (X. Chen).

<sup>\*</sup> Corresponding author.

#### 31-331.

More broadly, researchers have widely studied the SLS of PA12 powders via experimental analysis [34,35], numerical modeling and simulation [36,37], and combined experimental and numerical analysis [38,39]. Researchers have also explored methods to obtain better mechanical properties of the printed parts [40], to investigate the effects of particle shape, size, or process parameters on part properties [41], to test the fatigue behaviors for powders and specimens [42], and to optimize processing parameters [36]. However, for material aging and reuse in SLS, prior research focused on scattered subsets of a complex problem: for instance, the mechanism of powder deterioration [18,19], the flowability of powders [20,24,25], part microstructures [19], part mechanical properties [27,28] and parameter settings in SLS [31-33]. A heuristic overview of the state-of-the-art does not yet exist to reveal the complex material aging and its impact in SLS. Such an effort is particularly important for industries to standardize manufacturing protocols with a clear understanding of the underlying science and potential tradeoffs [43-45]. With the potentials of SLS and additive manufacturing on the one hand, and the limited results of material aging in SLS on the other, this paper reviews comprehensively research on aging mechanisms and degradation behaviors of PA12 powders in SLS. Exploring the nature of material degradations, this survey contributes to the field by (1) associating material characteristics with 3D printed parts, (2) relating manufacturability with such characteristics of the reused materials as particle size/sphericity, microstructure, material flowability and viscosity, and (3) exploiting the relationships between powder size/sphericity, surface morphology, microstructure and part roughness/dimensional-accuracy. Whenever possible, we tested the trend analysis through experimentation on hardware in the authors' laboratory, and we provide recommendations on machine control based on the test results.

# 1.1. Outline of this review

We will first introduce the SLS process and the related polymeric materials, followed by the aging behavior and aging mechanism of PA12

powders in SLS. Due to aging, recycled PA12 powders differ from new powders both microcosmically and macrocosmically. Fig. 1 summarizes the major changes, including powder property changes, part property changes, and parameter settings when using aged PA12 powders in SLS. For powder property changes, we will cover particle size/shape distributions, surface morphology, microstructures, thermo-chemical properties, and flowability through comparing new and reused PA12 powders. In addition, we will investigate the property changes of SLS parts 3D printed using aged powders. Categories of changes here will include part surface morphology, microstructures, thermo-chemical properties, density, tensile strengths, Young's modulus, and elongations at break. To gain more insights on the principles of parameter setting when using aged powders in SLS, we will survey predominant process parameters, such as pre-heating temperature, energy density, and layer thickness, etc. This paper will also research the correlations between parameter setting and part properties.

We organize the structure of the review as follows. Section 2 describes the SLS process and the related polymeric materials. Section 3 presents the aging behavior and aging mechanism of PA12 powders in SLS. Section 4 shows the property changes of aged PA12 powders. We exhibit property changes of parts 3D printed using aged PA12 powders in Section 5. In Section 6, we study the key parameter settings when using aged PA12 powders.

# 2. The SLS process and the related polymeric materials

A typical object in SLS is built from thin layers of powder materials. During the solidification of each layer, a high-power laser moves at several meters per second to form a microscopic melt pool, and selectively sinter/melt the particle powders (step <3> in Fig. 2). After consolidation, the powder bed lowers by the thickness of a new thin layer (step <4> in Fig. 2). New powders are then spread over the current deposit to start the next repetition (steps <1> and <2> in Fig. 2).

In SLS, three types of commonly used polymers are thermoplastics, thermosets, and elastomers, wherein thermoplastics are the most popular due to their high mechanical performance, chemical resistance, and

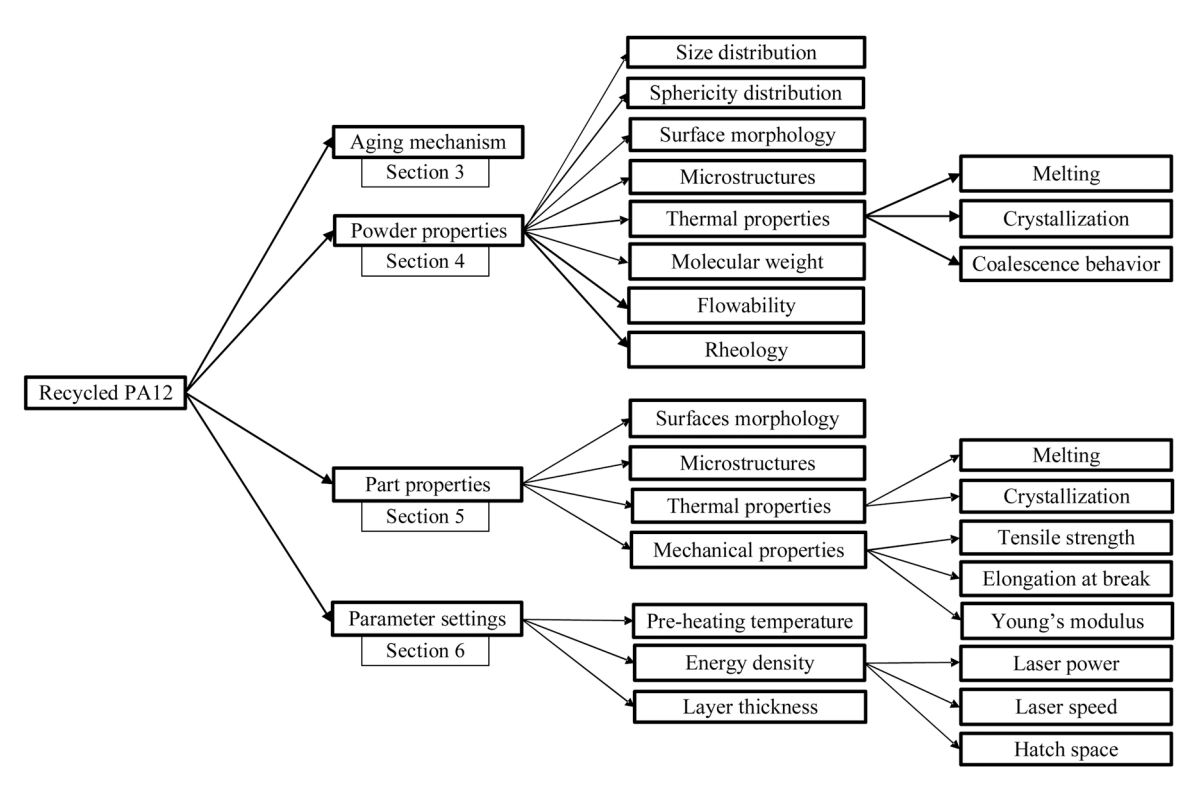


Fig. 1. The aging behavior of PA12 powders in the SLS process.

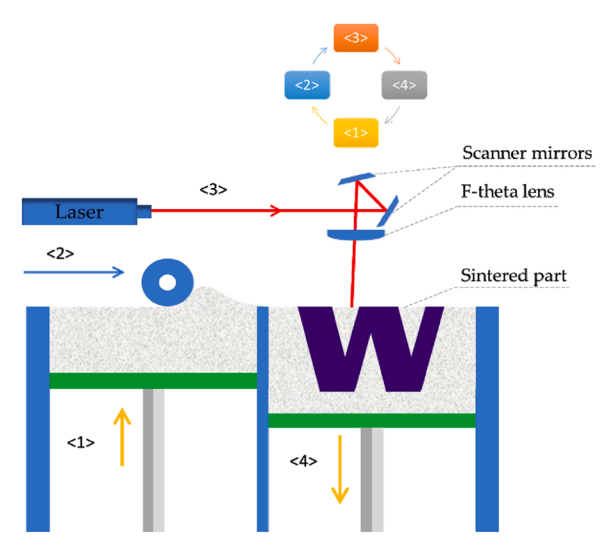


Fig. 2. Illustration of the SLS process.

excellent recyclability [46,47]. Thermoplastics mainly include amorphous polymers such as polycarbonates (PCs), and semi-crystalline polymers, such as nylons (polyamide) [11]. In particular, semi-crystalline polymers have proved to be more suitable for high-strength functional prototypes in SLS than amorphous polymers [48,49]. Among the semi-crystalline polymers, PA12 has attracted converging interests due to its suitability, ease of processability (i.e., broad sintering window), stability, dimensional accuracy, superior chemical and physical properties [50,51].

# 3. Aging behavior and aging mechanism of PA12 powders in the SLS process $\,$

#### 3.1. Microstructure of new PA12 powders

The microstructures of PA12 (semi-crystalline polymers) consist of amorphous regions and crystalline regions, and the molecule structure of PA12 is a combination of carbon atoms with the amide group (-NHCO-) [21]. The typical crystal structure of PA12 exhibits both  $\alpha$  and  $\gamma$  phases. The polymer chains in the  $\alpha$ -form are oriented in an unparallel way. In the more stable  $\gamma$ -form with a hexagonal crystal structure, chains are oriented in parallel [18,52]. The  $\alpha$ -form contributes to the brittleness of the crystal, while the  $\gamma$ -form enhances the toughness due to the twisted helical conformations around amide segments. The chain flexibility of the semi-crystalline polymer increases as more amide groups are present. The crystalline and amorphous regions determine the toughness of the polymer because of the irregular arrangement of the molecule chains.

At the molecular level, new PA12 powders contain long molecular chains. The chains form by linking the PA12 monomers together through the polycondensation reaction with the by-product  $H_2O$  (Fig. 3a). In the

long molecular carbon chains, a PA unit (Fig. 3b) consists of 11 methylene groups (in a linear chain) linked by an amide group, forming the basic chemical microstructure of the original PA12 powders.

#### 3.2. Aging behavior of PA12 powders

Various grades of PA12 powders from different suppliers are used in SLS. New powders go through complex thermal histories during powder coating, energy absorption, material consolidation, and cooling [53]. Only a small part of the new powders is sintered (e.g., 10~20%) during SLS [19,20]. A majority of powders remain unmolten and can be reused theoretically. Due to the heating and cooling cycles, both the physical and chemical properties of the unmolten PA12 powders change. Such changes are referred to in this review as powder aging. In general, aging negatively impacts powder shape, microstructures, chemical components, molecular chains, flowability, and viscosity. Vacuum and nitrogen atmosphere both reduce oxidative reactions that exacerbate powder aging [24]. Also, during sintering, the unused PA12 powders remain at elevated temperatures below the melting point for an extended period. This creates a denser crystal morphology to increase the melting point of the powder, and increases the chain length due to solid-state polycondensation [18]. The paper will survey quantitively the intensity of PA12 material aging, aging behavior/mechanism, and effects of aging on powder/part/process parameter.

# 3.3. Aging mechanism of PA12 powders

The aging mechanism of PA12 powders is complex and covers a series of physical and chemical degradations. We summarize and evaluate

**Table 1**Aging mechanism of PA12 powders in SLS.

| Item                   | Aging mechanism   |  |  |
|------------------------|---|--|--|
|                        | Physical degradation[21,28, 53,54]  | Chemical degradation[13,18, 54–56,59]  |  |
| Reversibility          | Reversible[53]  | Irreversible[54]   |  |
| Role                   | Secondary   | Dominant[19,59]  |  |
| Cause                  | Thermal load/High temperature[54]   | High temperature/Oxygen/<br>Laser  |  |
| Mechanism              | <ul> <li>Relaxation of orientations</li> <li>Agglomeration</li> <li>Post-crystallization</li> </ul>   | <ul> <li>Thermal oxidation</li> <li>Solid-state post-condensation</li> <li>Brill Transition of peak merging</li> <li>Hydrolysis</li> </ul>                         |  |
| Effects on<br>material | <ul> <li>Concentration change</li> <li>Particle aggregation</li> <li>Spherulites growth/<br/>structure</li> <li>Increased crystallization<br/>degree</li> <li>Increased lamellae<br/>thickness</li> </ul> | <ul> <li>Molecular chain scission</li> <li>Molecular cross-linking</li> <li>Chain branching</li> <li>Chain lengthening</li> <li>Thermal property change</li> </ul> |  |

$$\begin{array}{c} O & O & O \\ II & II \\ H-[HN(CH_2)_{11}C]_m-OH+H-[HN(CH_2)_{11}C]_n-OH \longrightarrow H-[HN(CH_2)_{11}C]_{m+n}-OH+H_2O \\ \\ & (a) \ Dehydration \ polycondensation \ reaction \ of \ PA12 \\ & & & & & & & \\ & & & & & & \\ & & & & & & \\ & & & & & & \\ & & & & & & \\ & & & & & & \\ & & & & & & \\ & & & & & & \\ & & & & & & \\ & & & & & & \\ & & & & & \\ & & & & & \\ & & & & & \\ & & & & & \\ & & & & & \\ & & & & & \\ & & & & & \\ & & & & & \\ & & & & & \\ & & & & \\ & & & & & \\ & & & & \\ & & & & \\ & & & & \\ & & & & \\ & & & & \\ & & & & \\ & & & & \\ & & & & \\ & & & & \\$$

Fig. 3. (a) Dehydration polycondensation reaction of PA12, and (b) PA12 unit.

the physical and chemical degradations in Table 1. Physical degradation is a reversible process, occurring under thermal load/high temperature, and leading mainly to relaxation of orientations, concentration changes, agglomeration, and post-crystallization [28,53,54]. Post-crystallization results in increased crystallization degree, increased lamellae thickness, crystal structure change and spherulites growth. With crystal structure changing, material has shrinkage and warpage. Through spherulites growth, irregular chains begin to form regular chain-folded structures [21]. Aside from the physical degradation, irreversible chemical degradation dominates in the aging process. Generally, chemical degradation changes the chain structures of polymers through chain scission, cross-linking, lengthening or branching resulted from oxidation, hydrolysis, and post-condensation [13,54-56]. These behaviors lead to more significant differences between new and aged powders [57]. Previous works have identified that thermal oxidation, solid-state post-condensation, and Brill Transition of peak merging are three main chemical degradation mechanisms of PA12 in SLS [18,19,40, 58]. We explain, compare and evaluate these three mechanisms in the following sections.

# 3.4. Main chemical aging mechanisms

#### 3.4.1. Thermal oxidation

Even with a controlled-environment chamber filled with nitrogen, oxygen remains in the SLS building chamber (e.g., 2–5% [19,60]). Such process imperfections, together with the high chamber temperature and laser radiations, lead to thermal oxidations of the PA12 powders. Both the chemical structure and the molecular chain change in the laser-induced thermo-oxidative degradation (Fig. 4a). In each PA12 unit described in Fig. 3b, C-H bonds adjacent to nitrogen are weak and easy to be oxidized. During laser radiations, free hydrogen radicals emerge from these carbons. Consequently, most oxidation reactions occur on the carbons adjacent to nitrogen [61–63]. Previous FTIR (Fourier-transform Infrared Spectroscopy) studies revealed the existence of infrared bands at 1368, 1158, 1062, and 946 cm<sup>-1</sup> in new powders, assignable respectively to C-H bending, CH<sub>2</sub> twisting, skeletal motion involving CONH, and CONH in-plane motion [64–66]. Such spectral peaks are

found to dramatically diminish or even disappear after the sintering process [18], indicating that amide groups get oxidized on carbons adjacent to nitrogen. With 8-time reuse, C-H bonds close to nitrogen decreases by 50% [63].

Generally, free molecule radicals emerge from the decomposition of PA12 and initiate oxidative reactions [19,59]. In the propagation reactions, oxygen is added and transferred to the unstable structures or middle products (e.g.: peroxide radicals and peroxide). The termination reaction occurs, in the end, to form stable final products or structures to complete the oxidation reaction. The following equations capture the basic autoxidation scheme (BAS) of PA12 [67,68]:

$$PH (Polymer) \to P \bullet \tag{1}$$

$$P \bullet + O_2 \to PO_2 \bullet \tag{2}$$

$$PO_2 \bullet + PH \rightarrow P \bullet + POOH$$
 (3)

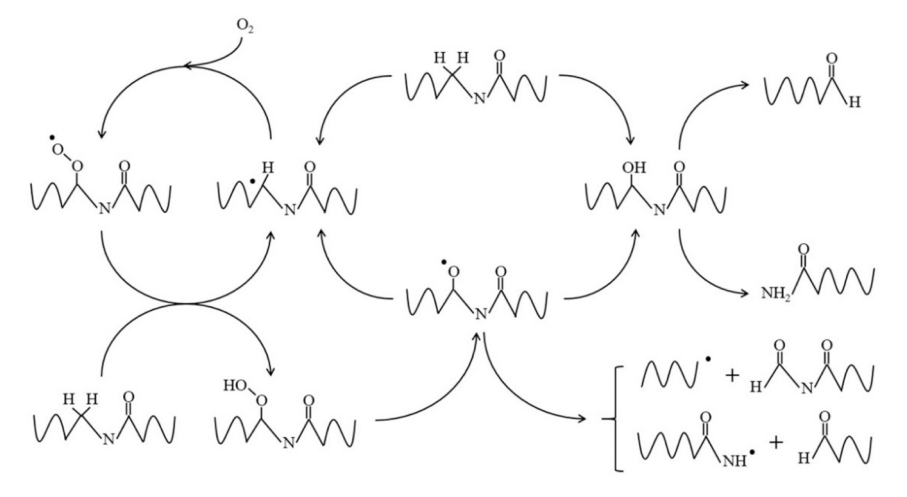
$$P \bullet + P \bullet \rightarrow \text{final product}$$
 (4)

$$P \bullet + PO_2 \bullet \rightarrow \text{final product}$$
 (5)

$$PO_2 \bullet + PO_2 \bullet \rightarrow \text{final product} + O_2$$
 (6)

For the laser-induced thermo-oxidative degradation in SLS (Fig. 4a), intensive laser radiation and the high temperature initiate the degradation reaction of PA12 materials to dehydrogenize and form alkyl radicals. Alkyl radicals later combine with oxygen (O<sub>2</sub>) to form peroxy radicals. The peroxy radicals further capture hydrogen atoms from the PA12 monomers to produce alkyl radicals and hydroperoxides [18]. Under the laser radiation and elevated temperature, the hydroperoxides lose the hydroxide radicals to create the new radical group with oxygen on both sides of nitrogen. The new radical group then forms the stable structure with two carbon and oxygen double bonds (Fig. 4b), which are the chemical structure of the aged PA12 monomer. Besides, the new radical group also sometimes reacts to form alkyl radicals for circular reactions.

Accompanied by thermal oxidation, molecular chain cross-linking and scission occur simultaneously [69]. Different from the micro-scale changes of thermal oxidation, chain cross-linking and scission are



(a) Laser-induced thermo-oxidative degradation reactions [18] (with permission from publisher)

$$+ \bigvee \bigvee_{N} \bigvee_{N} \bigvee_{J_{\overline{n}}} \downarrow_{\overline{n}}$$

(b) Aged PA12 unit

Fig. 4. Thermal oxidation mechanism of PA12 powders.

macro-molecular behaviors. Either cross-linking or scission can be the predominant process with thermal oxidation, depending on material type, oxygen content, and time duration at elevated temperature. For the PA12 SLS process, chain cross-linking is found to be the predominant phenomenon due to the nitrogen atmosphere [24].

# 3.4.2. Post-condensation and Brill Transition of peak merging

In addition to the thermo-oxidative degradation, solid-state/melt-state post polycondensations is another irreversible degradation mechanism of PA12 [18,23,70]. Polycondensation is a polymer synthesis process. In detail, PA12 chain ends with -H and -OH bonds, and at normal atmosphere, they randomly react with each other to produce  $\rm H_2O$ . The reaction is reversible, and  $\rm H_2O$  reacts with the other ends of -H and -OH bonds to form new  $\rm H_2O$ . This process is in dynamic equilibrium to keep the average molecular length/molecular weight of PA12 stable [13]. In the SLS process with high temperature and laser radiation, the water vapor reduces and the polycondensation process is accelerated. This atmosphere breaks the dynamic equilibrium, and enhances the formation of long molecular chain/increased molecular weight [13,67,71].

Brill Transition of peak merging, a solid-state crystalline transition driving by crankshaft motions in chain [72,73], was found for PA12 polymer aging or heating. When temperature is near the melting point, the diffraction peaks of PA12 powder change in the X-Ray Diffraction (XRD) profiles [18]. In particular, one reflection peak shifts close to the other, causing the other peak to become more indistinguishable; eventually, the two peaks merge into one single peak. The reason for this phenomenon is that, during aging or heating to around the melting point, the main crystal structures of PA12 transform from α-phase to the more stable  $\gamma$ -phase [73,74]. Induced by the high temperature, the main mechanism of the crystal phase transformation is the conformational changes to sufficiently twist methylene units [72]. From FTIR, spectra of the methylene sequences change gradually as aging continues and temperature increases. The bands at 1343, 1289, and 1223 cm<sup>-1</sup> become weaker and more disordered, eventually disappearing [75]. Aging time and temperature significantly affect the Brill Transition. Besides, the interplanar spacing and hydrogen bonding between neighbor molecular chains also influence the Brill Transition.

# 3.4.3. Comparison

Table 2 compares the main chemical degradation mechanisms of PA12 in SLS. Thermal oxidation always dominates the aging with high temperature/oxygen, and greatly influences various material properties. The laser was verified to have at least 4-time stronger effects than

oxygen on PA12 thermal oxidation [59]. Solid-state/melt-state post polycondensation is secondary in aging caused by reduced water vapor, mainly affecting chain length and molecular weight. The Brill Transition of PA12 in SLS is weak, occurs at high temperature, and influences material microstructure/crystalline.

#### 4. Property changes of aged PA12 powders

#### 4.1. Particle size/sphericity distribution

Particle size distribution affects process and part property deviations, such as part surface roughness and porosity [14,76]. In general, part roughness increases because of the broader particle size distribution resulting from small particle agglomeration. Bigger gaps between particles lead to increased part porosity. Several studies argued that compared to the new powders or 50%-50% new-aged mixed powders, particle sizes barely change after aging and remain approximately a Gaussian distribution centered at  $50-60~\mu m$  [19,26].

Particle sphericity (0.00-1.00) measures how closely the shape of a particle approaches a perfect sphere (sphericity=1.00). Fig. 5 presents the obtained sphericity distributions of study using the EOS GmbH PA12 [43]. The tests show that the percentage of particles with sphericity 0.9–1.0 is 21% in new powders, in contrast to 16% in aged powders (aged at 171 °C after standard SLS processes on an EOS P 390 machine). Mielicki's work [14] obtained a similar conclusion using EOS GmbH PA12, showing that the sphericity of around 4.5% PA12 particles decreased from 0.9 to 0.75 with 120 h of aging (aged at a temperature of 174 °C in a vacuum VT 6060 P-400, Thermo Scientific oven).

# 4.2. Particle surface morphology

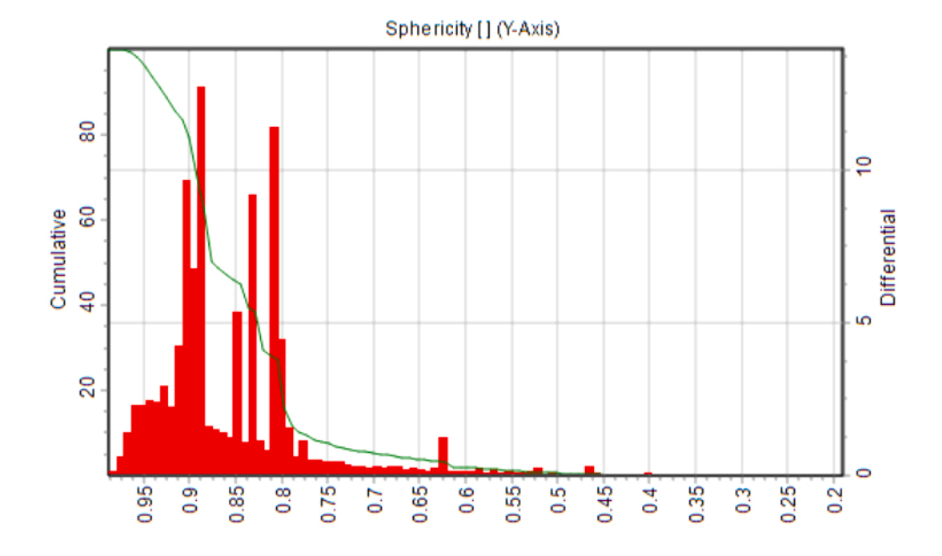
In SLS, PA12 powders are exposed to a long period of heating cycles during the pre-heating and sintering processes. These processes accelerate the evaporation of moisture or alcohol inside the powders. Moreover, combined with recycling and repeated expansions/shrinkages in the heating and cooling cycles, surface morphology of aged PA12 powders shows 3%-5% increased cracking or fragmentation [18,19,26, 43]. An example is shown in Fig. 6.

# 4.3. Particle microstructures

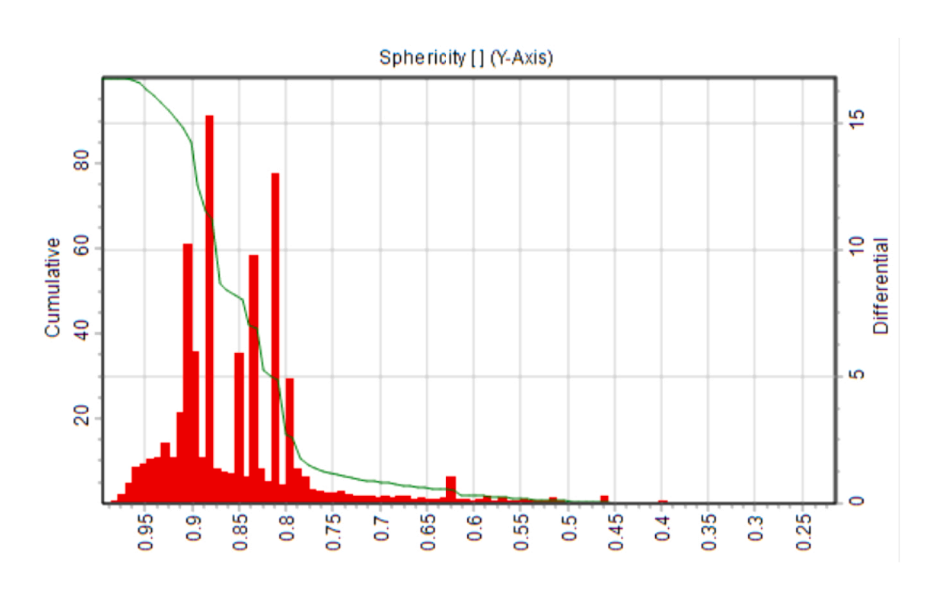
In the crystalline region, microstructures of aged PA12 particles exhibit significant differences compared to new particles. For aged PA12, post-crystallization process starts to form spherulite structures

**Table 2**Comparisons between main chemical degradation mechanisms of PA12 in SLS.

| Item                | Main chemical degradation mechanisms                               |   |                                      |  |
|---------------------|--|---|--------------------------------------|--|
|                     | Thermal oxidation[18,61–63]  | Post condensation[13,23,71]                               | Brill Transition[18,72,73]           |  |
| Role                | Primary[19,59]   | Secondary   | Weak                                 |  |
| Cause               | <ul> <li>High temperature</li> </ul>                               | <ul> <li>High temperature</li> </ul>                      | <ul> <li>High temperature</li> </ul> |  |
|                     | <ul> <li>Oxygen</li> </ul>   | • Laser   |                                      |  |
|                     | • Laser  |   |                                      |  |
| Mechanism           | Thermal oxidation[67,68]   | Enhanced synthesis[13]                                    | Peak merging[72,73]                  |  |
| Before aging        | $     \begin{array}{ccc}                                   $       | H-[HN(CH <sub>2</sub> ) <sub>11</sub> C] <sub>n</sub> -OH | (200) (010)                          |  |
| After aging         | $+ \bigvee \bigvee_{N} \bigvee_{N} \xrightarrow{J_{\overline{n}}}$ | H-[HN(CH $_2$ ) $_{11}$ C] $_{m+n}$ -OH                   | (001)                                |  |
| Effects on material | Chain structure  | <ul> <li>Chain length</li> </ul>                          | Microstructure                       |  |
|                     | <ul> <li>Chain cross-linking</li> </ul>                            | <ul> <li>Molecular weight</li> </ul>                      | <ul> <li>Crystalline</li> </ul>      |  |
|                     | <ul> <li>Chain scission</li> </ul>                                 | <ul> <li>Crystalline</li> </ul>                           |                                      |  |



# (a) New powders



(b) Aged powders

**Fig. 5.** Particle sphericity distribution of new PA12 powders and aged PA12 powders [43]. (with permission from publisher).

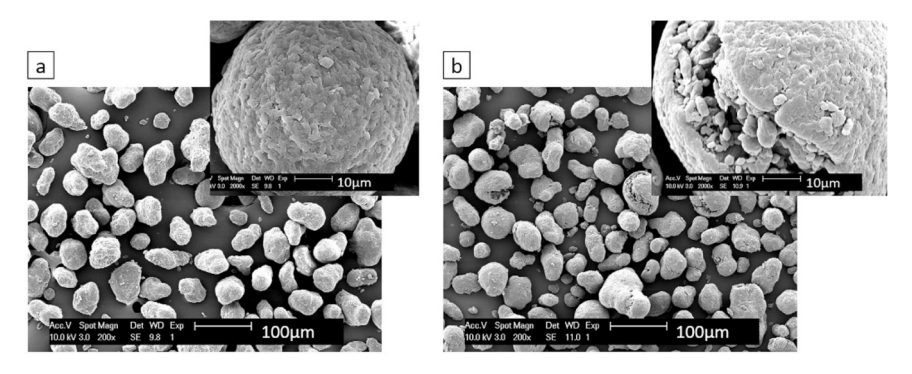


Fig. 6. Scanning electron microscope (SEM) images of (a) new and (b) aged PA12 powders in SLS [19]. (with permission from publisher).

when cooling down from the pre-heating temperature. Firstly, nucleation occurs to form spherulite sites for spherulite growth. With temperature reducing, spherulites start to grow, then radiate from the central regions of the spherulite core, and form spherical structures eventually [13,77]. This behavior leads to spherulite aggregation and crystallite formation.

When temperature is between the pre-heating temperature and the glass transition temperature, the mobility of the molecular chains increases. Free radicals form, attracting nearby molecular chains and other free radicals to form longer and more complex spherulite structures. The longer the powders stay under the heating and cooling cycles, the more complex the spherulite structures become. Thus, in- and post-process aging lead to rapid spherulites growth, dense spherulite structures (Fig. 7a), and high crystallinity of the particle materials. This explains why the microstructure of the aged powders appears to be more complex than new ones [19,21]. It is also noteworthy that recycled PA12 powders have more spherulite structures to spread. Therefore, recycled PA12 has a regular chain-folded state (Fig. 7b right) to save space while the new powders exhibit an irregular state (Fig. 7b left) [21].

# 4.4. Thermo-chemical properties

Thermo-chemical properties of PA12 powders directly influence particle bonding and fusion in SLS, hence are crucial to degradation and reusability. This subsection evaluates key changes in melting and cooling behaviors after PA12 aging, along with insights into the underlying mechanisms and different causes of the changes.

The powder melting/crystallization are usually evaluated by the Differential Scanning Calorimetry (DSC) technology [18,19,23,50]. Typical DSC graphs with specific heat flow consists of both heating and cooling cycles for semi-crystalline thermoplastics. Melting is endothermic since we have to provide energy to the system, the opposite for crystallization (Fig. 8) [50]. Crystallization during processing inversely impacts SLS feasibility. To inhibit crystallization, the material temperature is kept between melting and crystallization temperatures [50].

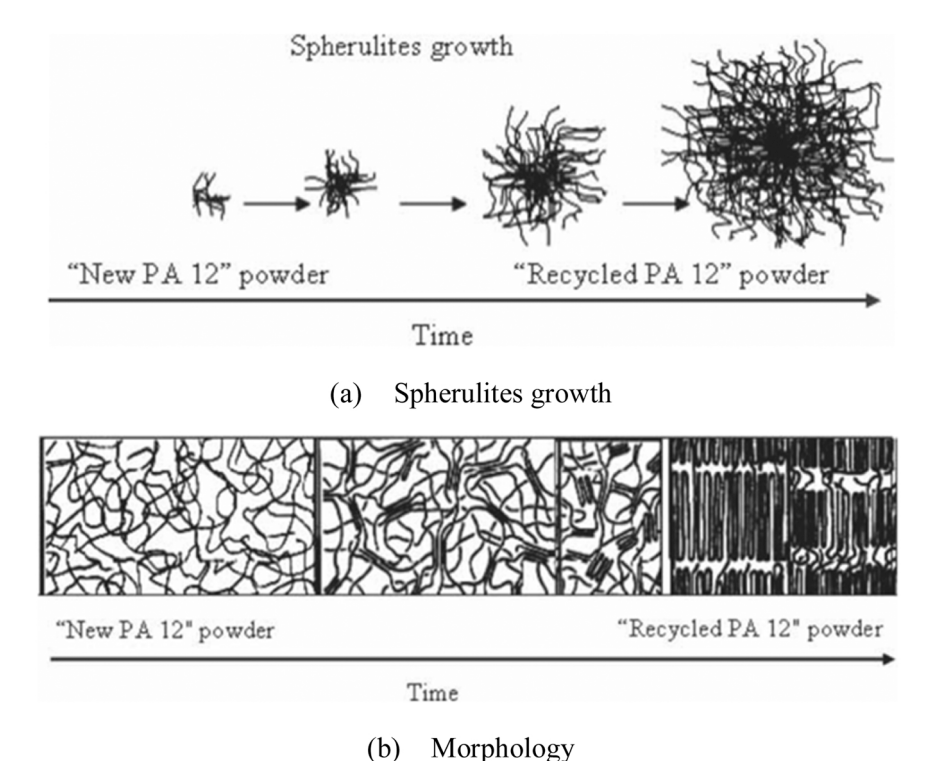
This is critical to ensure proper adhesion between sintered layers, overall part dimensional stability, and to prevent unused powder from melting around the sintered part.

# 4.4.1. Thermo-chemical property changes

Compared to the new powders, aged PA12 powders demonstrate noticeable changes in powder melting and crystallization. For EOS GmbH PA12 processed on a DTM Sinterstation 2000 with CO<sub>2</sub> laser (optimal parameters: pre-heating temperature 170 °C, laser power 5 W, scanning speed 600 mm/s, scan spacing 0.3 mm, and layer thickness 0.15 mm), a broadened melting trajectory appears in the heating process of aged powders [19]. It indicates an increased melting shoulder interval, defined as the temperature ranges between the start and final melting points. The melting shoulder interval of aged EOS PA12 is 10.8 °C, while that of new EOS PA12 is 7.9 °C [19].

For VESTOSINT X1556, Evonik PA12 processed on the HK P320 SLS system (optimal parameters: pre-heating temperature 167 °C, laser power 18 W, scanning speed 4000 mm/s, scan spacing 0.3 mm, and layer thickness 0.1 mm), the aged PA12 shows the wider sintering window, defined as the temperature interval between onset melting and onset crystallization [26]. The sintering window of aged PA12 is 31 °C, while that of new PA12 is 29.96 °C [26]. Meanwhile, using the same SLS system and processing parameters, the melting enthalpy and crystallization enthalpy of VESTOSINT X1556, Evonik aged PA12 decrease [18]. The melting enthalpy of VESTOSINT X1556, Evonik aged PA12 is 80.71 J/g, and that of new is 96.62 J/g [18]. The crystallization enthalpy of Evonik aged PA12 is 42.13 J/g in comparison to 45.03 J/g of new PA12. The changes are ascribed to the formation of more stable molecular chains with two carbon and oxygen double bonds.

To gain more insights, we conducted DSC tests with a TA Instrument DSC Q20 and EOS PA12 powders, following the test sequences: heating, cooling, and reheating [44]. The aged EOS PA12 was reclaimed from an EOS P 390 SLS machine (optimal parameters: pre-heating temperature 171  $^{\circ}$ C, laser power 40 W, scanning speed 2800 mm/s, scan spacing 0.3 mm, and layer thickness 0.15 mm). The first heating cycle in DSC



(b) Morphology

**Fig. 7.** The comparison of spherulites growth and morphology between new and recycled PA12 powders [21]. (with permission from publisher).

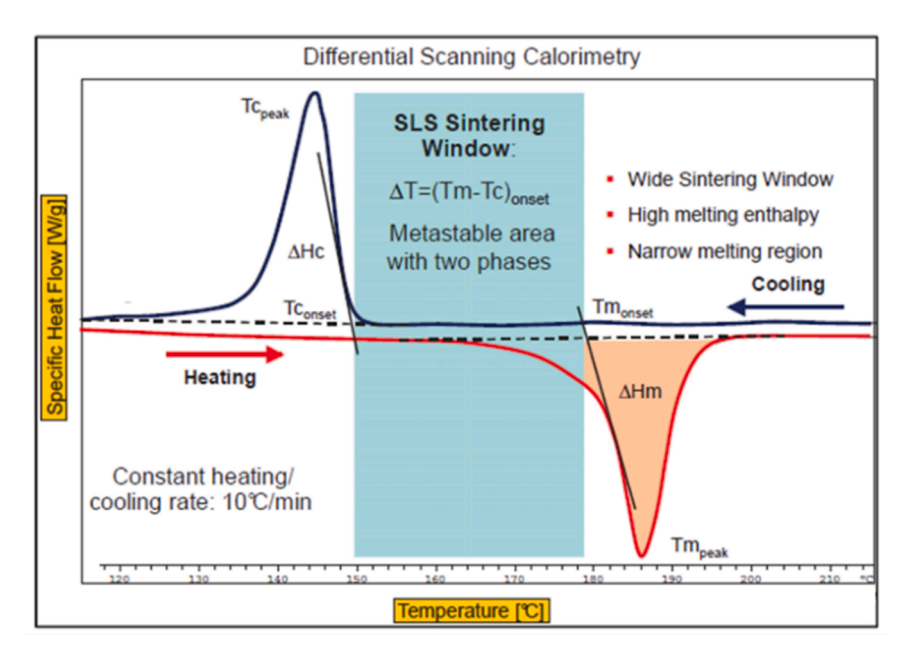


**Fig. 8.** Typical DSC-Thermograms in SLS process [50]. (with permission from publisher).

curve presents that the onset melting temperature of aged powder has a mild decrease (aged:  $181.81\,^{\circ}$ C, new:  $183.36\,^{\circ}$ C) [44]. However, the peak melting temperature of aged powders increases (aged:  $188.18\,^{\circ}$ C, new:  $186.38\,^{\circ}$ C) as well as the melting enthalpy (aged:  $101.3\,$ J/g; new:  $92.1\,$ J/g), which is different from the VESTOSINT X1556, Evonik PA12. Table 3 exhibits thermo-chemical property changes between new and

 $\begin{tabular}{ll} \textbf{Table 3} \\ \textbf{Thermo-chemical property changes between new and aged PA12 powders of different grades.} \\ \end{tabular}$ 

| (a) PA12, EOS GmbH[19,44]          |                    |             |  |
|------------------------------------|--------------------|-------------|--|
| PA12 grade                         | PA12, EOS GmbH     |             |  |
|                                    | Before aging       | After aging |  |
| Melting shoulder interval          | 7.9 °C             | 10.8 °C     |  |
| Sintering window                   | 25.7 °C            | 27.7 °C     |  |
| Onset melting temperature          | 183.36 °C          | 181.81 °C   |  |
| Peak melting temperature           | 186.38 °C          | 188.18 °C   |  |
| Melting enthalpy                   | 92.1 J/g           | 101.3 J/g   |  |
| Onset crystallization temperature  | 152.14 °C          | 150.40 °C   |  |
| Peak crystallization temperature   | 148.23 °C          | 146.48 °C   |  |
| Crystallization enthalpy           | 50.15 J/g          | 48.42 J/g   |  |
| (b) VESTOSINT X1556, Evonik[18,26] |                    |             |  |
| PA12 grade VESTOSINT X1556, Evon:  |                    | vonik       |  |
|                                    | Before aging       | After aging |  |
| Sintering window                   | 29.96 °C           | 31 °C       |  |
| Peak melting temperature           | 182.37 °C          | 182.68 °C   |  |
| Melting enthalpy                   | 98.24 J/g          | 92.56 J/g   |  |
| Peak crystallization temperature   | 141.45 °C          | 143.24 °C   |  |
| Crystallization enthalpy           | 45.03 J/g          | 42.13 J/g   |  |
| (c) Sinterit PA12 gray[63]         |                    |             |  |
| PA12 grade                         | Sinterit PA12 gray |             |  |
|                                    | Before aging       | After aging |  |
| Sintering window                   | 18.26 °C           | 19.83 °C    |  |
| Onset melting temperature          | 173.72 °C          | 175.61 °C   |  |
| Peak melting temperature           | 180.15 °C          | 180.49 °C   |  |
| Melting enthalpy                   | 108.80 J/g         | 99.94 J/g   |  |
| Onset crystallization temperature  | 155.46 °C          | 155.78 °C   |  |
| Peak crystallization temperature   | 152.40 °C          | 153.07 °C   |  |
| 0 111 11 11 1                      |                    |             |  |

54.39 J/g

Crystallization enthalpy

aged PA12 powders of different grades.

The melting temperature of the crystalline polymer is largely affected by the lamellae thickness in the crystallization region. The deceased onset melting temperature of the reclaimed EOS GmbH PA12 may result from the decreased lamellae thickness in the crystallization region. Due to the physical degradation, more particles aggregate with each other. These particles are more difficult to melt, increasing peak melting temperature and melting enthalpy.

Due to increased chain length in the aged powder promoted by melt-state polycondensation, the chain mobility decreases in the molten state. As a result, lower crystallinity (VESTOSINT X1556, Evonik PA12; aged: 44.22%; new: 46.94% [26]) and lower crystallization temperature (EOS GmbH PA12; aged: 150.40 °C; new: 152.14 °C [44]) is typically observed during cool-down. This phenomenon is clear from the reduction in the crystallization enthalpy in the aged powder (EOS GmbH PA12; aged: 48.42 J/g; new: 50.15 J/g [44]). The reduction is further enhanced in subsequent reuse of the powder. Chen et al. show a reduction in crystallinity from 46.2% to 38.6% after the fourth recycling [18].

It is worth mentioning that, though references [18,26] claimed the crystallinity reduction after reuse, references [19,21] reported increased crystalline ratios with reuse. The main reason for this divergence is that the researchers performed the experiments using PA12 from different vendors. The VESTOSINT X1556, Evonik PA12 was used in references [18,26], and the EOS GmbH PA12 was applied in references [19,21]. The results suggest that PA12 material crystalline ratios after reuse may increase or decrease, depending on the source of materials, the fabricating technologies, the producing environment, and the types of additives.

# 4.4.2. Thermo-chemical properties influenced by pre-heating temperature and build time

Considering that the whole SLS fabrication process is an aging process for the materials to be reclaimed, the increased pre-heating temperature and build time influence and even cause more severe material degradations, therefore affecting material thermo-chemical properties.

4.4.2.1. Pre-heating temperature. Previous studies show that the increased pre-heating temperature influences the thermo-chemical properties of aged PA12 powders [23]. When using EOS GmbH PA12

50.48 J/g

and a research SLS system (processing parameters: laser power 7.8 W, scanning speed 904 mm/s, scan spacing 0.25 mm, layer thickness 0.1 mm), different pre-heating temperatures of 164, 168 and 172 °C were applied [23]. Specifically, the onset and peak melting temperatures remains nearly unchanged when increasing the pre-heating temperature by 4 °C, while the melting enthalpy decreases by 5–10 J/g. A mild increase of the pre-heating temperature causes minimal degradations, if detectable [32]. That is the reason for the unchanged onset and peak melting temperatures. However, the increase in molecular weight lowers the crystallinity, decreasing the melting enthalpy. Unlike the melting behavior, the pre-heating temperature largely affects the crystallization behavior of materials. Increasing the pre-heating temperature by 4 °C results in a delay of the onset and peak crystallization temperatures by 2 °C, as well as a decrease of the crystallization enthalpy by 3 J/g.

4.4.2.2. Cumulative build time. Besides, the cumulative build time also affects the thermo-chemical properties. The influence of build time on melting behavior relies greatly on the sintering systems [21,23]. When using EOS GmbH PA12 and a Sinterstation 2000 SLS system (pre-heating temperature 172 °C), different build times were applied [23]. As the cumulative build time increases by 26.6 h, different systems cause the unchanged or increased onset and peak melting temperatures as well as decreased melting enthalpies [23]. The increase of the melting temperature and decrease of melting enthalpy originate from the post-crystallization or recrystallization effects [21]. Post-crystallization appears as the rise of crystallization ratio, while recrystallization relates to the transfer of crystalline structures. Both phenomena occur when cumulative build time increases. However, it remains unknown which one is predominant. As for the crystallization behavior, a cumulative build time increased by 26.6 h brings forward the onset of crystallization temperature by 2 °C and increases the crystallization enthalpy by 3-5 J/g. Material crystallization behavior shows similar responses to different SLS machines [23].

Table 4 compares the thermo-chemical properties influenced by preheating temperature and cumulative build time. It shows that the increased pre-heating temperature and cumulative build time have different effects on material crystallization behaviors. The reasons for these differences are assessed as follows. The experiments studying the increased pre-heating temperature were performed on a research SLS system, while those studying the cumulative build time were conducted on a Sinterstation 2000 SLS system. These two SLS systems have many differences in the heating system, atmosphere, sintering, cooling, et. al. Besides, the building strategies of the experiments studying the increased pre-heating temperature include loading materials, recoating, preheating, sintering, and cooling, totaling 8.4 h, while those studying the cumulative build time were to repeat the 5.3 h of building multiple times totaling 26.6 h. Furthermore, the pre-heating temperature is the key parameter that affects material crystallization behaviors, and these experiments used different pre-heating temperatures. These differences cause complex aging effects on materials, leading to different crystallization behaviors.

#### 4.4.3. Coalescence behavior

Coalescence behavior represents the phase change of PA12 powders from a solid-state to the molten phase. Hot stage microscopy shows three stages (slow softening, fast coalescence, and molten phase) of the material coalescences [19]. For PA12 EOS GmbH, new powders always coalesce fast during the test: slow softening (from 160 °C to 180 °C), fast coalescence (at 190 °C), and molten phase (at 200 °C). However, aged powders show similar behavior with new ones initially, but need more time to form the molten phase at a higher temperature eventually: slow softening (from 160 °C to 180 °C), fast coalescence (from 190 °C to 210 °C), and molten phase (> 210 °C). The change in the aged powders is due to their stable chemical structure and numerous high melting points. Good coalescence is the prerequisite of uniform solidification. Uniform solidification is crucial to form smooth, dense surfaces and good mechanical properties [44].

#### 4.5. Molecular weight

# 4.5.1. Molecular weight with aging

The molecular weight of aged PA12 powders increases compared to new ones, and the gel permeation chromatography (GPC) analysis is usually applied to identify the molecular weight distribution [78,79]. The increased molecular weight of aged PA12 powder is caused by the chain cross-linking from thermal oxidation [19,24] and the accelerated post-polycondensation [32,80]. These effects make the material molecular chains longer, denser and more complex. The weight-average molecular weight  $(M_w)$  and number-average molecular weight  $(M_n)$ rise with the increased aging temperature and aging time [21]. For EOS PA12, when aged at 120 °C for 110 h, the weight-average molecular weight increased by  $0.4 \times 10^5$  g/mol compared to new material; when aged at 170 °C for 110 h, the weight-average molecular weight increased by  $2.5 \times 10^5$  g/mol; when aged at  $120 \,^{\circ}$ C for  $180 \, h$ , the weight-average molecular weight increased by  $0.6 \times 10^5$  g/mol [13]. The weight-average molecular weight and number-average molecular weight of EOS PA12 are respectively 76,950 g/mol ( $M_w$ , new), 38,800  $(M_n, \text{ new})$  and 926,500 g/mol  $(M_w, 3\text{-time recycled})$ , 111,000  $(M_n, 3\text{-time recycled})$ 3-time recycled) [21].

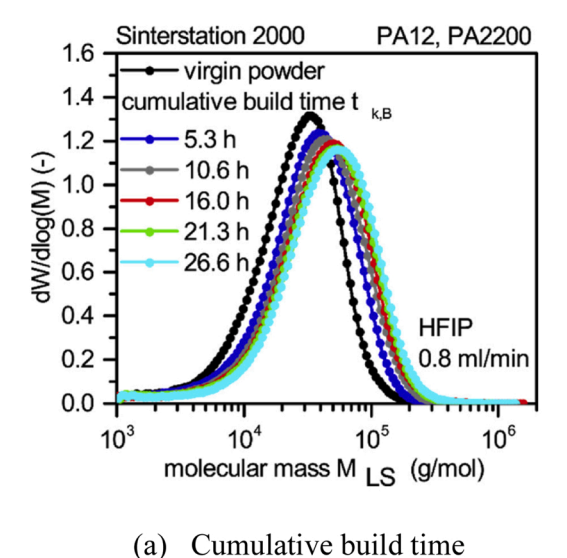
# 4.5.2. Molecular weight influenced by cumulative build time and preheating temperature

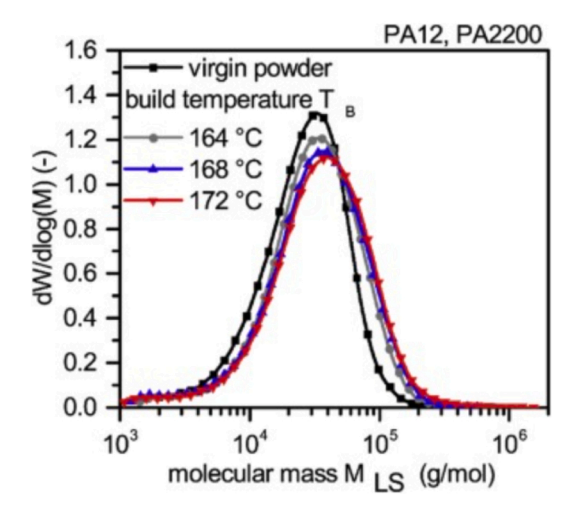
Cumulative build time is an important parameter affecting particle molecular weight distribution [23]. Fig. 9a presents effects of cumulative build time on average molecular weight of PA12. New powder shows average molecular weight of 32900 g/mol. With different build time of 10.6 and 26.6 h (applying the same preheating temperature), the average molecular weights are 49,400 g/mol and 61,100 g/mol [23]. A longer build time leads to a higher molecular weight.

Pre-heating temperature is another parameter affecting material molecular weight [21,80]. Fig. 9b presents effects of pre-heating temperature on average molecular weight of PA12. With different pre-heating temperature of  $164\,^{\circ}\text{C}$ ,  $168\,^{\circ}\text{C}$ , and  $172\,^{\circ}\text{C}$  (applying the same build time), the average molecular weights are 42,200, 45,500, and 49,700 g/mol [23]. A higher pre-heating temperature results in a larger molecular weight. However, the cumulative build time has larger

**Table 4**Comparisons between thermo-chemical properties influenced by pre-heating temperature and cumulative build time.

| Item                       |  |  | Pre-heating temperature increase by 4 $^{\circ}\text{C}$ [23]              | Cumulative build time increase by 26.6 hrs[21, 23]  |
|----------------------------|--|--|--|---|
| Thermo-chemical properties | Melting behavior  Crystallization behavior | Onset melting T Peak melting T Melting enthalpy Onset crystallization T Peak crystallization T | Unchanged Unchanged Decrease by 5–10 J/g Decrease by 2 °C Decrease by 2 °C | Unchanged or increase Unchanged or increase Unchanged or decrease Increase by 2 °C Increase by 2–4 °C |
|                            |  | Crystallization<br>enthalpy  | Decrease by 3 J/g  | Increase 3–5 J/g  |





# (b) Pre-heating temperature

**Fig. 9.** Effects of cumulative build time and pre-heating temperature on molecular weight of PA12 [23]. (with permission from publisher).

influences on material molecular weight than the pre-heating temperatures. The reason is that the pre-heating temperatures are controlled in a limited operation window around 170  $^{\circ}$ C to ensure process feasibility, while the ranges of the cumulative build time are normally much wider [23].

#### 4.6. Flowability

Good flowability is necessary to enable processibility of raw materials and deposition of the fabricated layers in SLS [81–83]. Previous works have reported to study the static/dynamic flow behaviors, and to improve the flowability of PA12 powders through adding  $\text{TiO}_2$  and silica [83–85]. Particle shape largely affects powder flowability [85]. Usually, particles with high sphericity show high flowability, while the irregular, potato-shaped, or rough-edged particles present low flowability.

Aging causes different effects on flowability of different PA12 powders. For EOS PA12, new powders exhibit good flowability and processability, while flowability of aged powders (reclaimed from an EOS P 390 SLS machine, processing parameters: pre-heating temperature 171 °C, laser power 40 W, scanning speed 2800 mm/s, scan spacing 0.3 mm, and layer thickness 0.15 mm) shows a significant decrease after degradations [43]. The decreased flowability adversely impact powder reuse/recoating. For Sinterit PA12 new powders, the basic flowability energy is 924 mJ, while that of 5-, and 8-time reused powders (reclaimed from a Sharebot SnowWhite SLS 3D printer, processing parameters: pre-heating temperature 160 °C, layer thickness 0.1 mm, and around 200 min for one printing) are 846, and 822 mJ [63]. Each reuse improves flowability of Sinterit PA12 by 1.5%.

# 4.7. Rheology

# 4.7.1. Viscosity

Due to degradations, aged PA12 powders have longer molecular chains, more complex chemical structures and increased molecular weight, largely influencing viscosity [18,19]. EOS PA12 was reported to have increased zero-shear viscosity after aging [13,19,86]. Moreover, a higher aging temperature or longer aging time lead to a larger viscosity [19]. The zero-shear viscosity of new EOS PA12 powder is  $5.20 \times 10^2$  Pa·s, while that of powders aged 20 h at 120, 150 and 170 °C are respectively  $1.51 \times 10^3$ ,  $7.50 \times 10^3$  and  $1.80 \times 10^5$  Pa·s [13]. At 190 °C, the zero-shear viscosity of EOS PA12 powder is around  $10^3$  Pa·s after 15 min of aging, and around  $10^4$  Pa·s after 30 min of aging [19,86].

Duraform PA12 has similar phenomena: the complex viscosity of new powders is around  $10^3$  Pa·s, and that of reused powder (aged at  $170\,^{\circ}$ C) is  $5.0\times10^4$  Pa·s [87]. The zero-shear viscosity of Orgasol PA12 has little change after aging 30 min at 190, 210 and 230 °C [86]. For the VESTOSINT X1556 PA12, the zero-shear viscosity increases first with reuse and then decreases (Fig. 10). The zero-shear viscosity increases after the first and the second times of reuse, and decreases after the third-time reuse [18]. These significant time-dependent zero-shear viscosity changes confirm that PA12 demonstrates melt-state polycondensation [18,70].

# 4.7.2. MVR and MFI

The other indexes to measure material rheological property are the melt volume rate (MVR) and the melt flow index (MFI). MVR is defined as the volume of a thermoplastic polymer, flowing in ten minutes through a capillary for alternative prescribed pressures and temperatures, cm<sup>3</sup>/10 min. MFI is expressed as mass of the polymer, in grams, flowing through a capillary under alternative prescribed pressures and temperatures in ten minutes, g/10 min. Measured in capillary rheometers, MVR [18,20,24,25,57] and MFI [78,88,89] can present

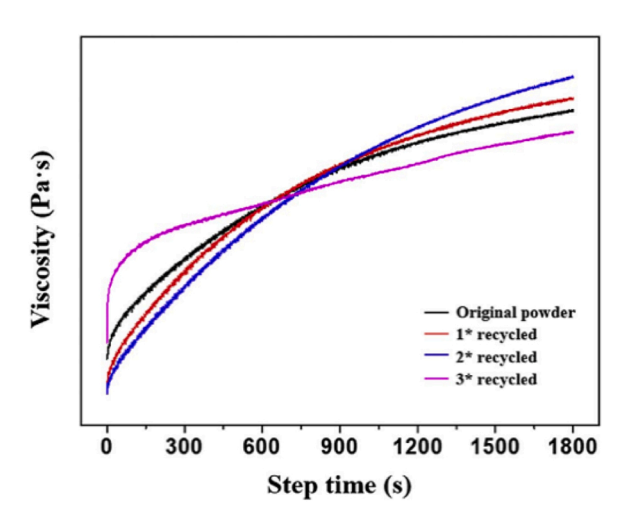


**Fig. 10.** Viscosity-time curves at 200 °C for the PA12 original and recycled powders [18]. (with permission from publisher).

degradation status of PA12 material in SLS. Generally, new powders have higher MVR and MFI values compared to aged powders. For DuraForm PA12, MFI of new powder is 52.01 g/[10 min], and that of waste powder is 20.38 g/[10 min] [16]. For EOS PA12, MFI of new powder is 50.1 g/[10 min]; MVR of 1-time, 2-time and 3-time reused powders are 28.90, 17.41, and 13.50 g/[10 min] [21]. Fig. 11 shows MVR values of EOS PA12 powders oven aged, and machine aged at 174 °C [24]. A longer aging time results in smaller MVR values (e.g.: in oven, MVR decreases from 65 cm³/[10 min] to 20 cm³/[10 min] with 120 h aging). This attributes to the longer molecular chain in aged powder caused by melt-state polycondensation. The increased chain length reduces chain mobility and increases flow resistance with reduced MVR/MFI. MVR and MFI are inversely proportional to viscosity. Table 5 compares the aging effects on material viscosity and MVR/MFI.

# 5. Property of parts using aged PA12 powders

When properties of the reclaimed powders allow for a successful SLS, the quality of the resulting manufactured parts defines the ultimate applications. The properties of part using aged PA12 powders, such as part microstructure, surface morphology, thermo-chemical property, crystalline structure evolution, and mechanical property, change compared to part using new powders. We will discuss these part properties in detail in this section. Notice that these changes typically follow a standard printing process in the comparison, i.e., the processing parameters are equal or close to the case with new powders [43–45].

#### 5.1. Surface morphology

Part dimensional accuracy and surface roughness are two common kinds of part surface morphologies and usually degrade when using reclaimed PA12 powders [18,90].

# 5.1.1. Dimensional accuracy

Since laser sintering is generally free-standing with no applied supports, dimensional accuracy of the 3D-printed part is a primary concern in SLS [91]. Uniform solidification is crucial to forming a part with accurate dimensions [85]. An important consideration to ensure uniform solidification is controlling sintering behavior. Laser energy density and pre-heating temperature are key factors affecting sintering behavior [92]. Laser energy density greatly influences the combination of adjacent particles: insufficient energy density leads to poor coalescence, while excessive energy density results in severe degradations. Certainly, laser only supplies part of the total energy deposited into the materials.

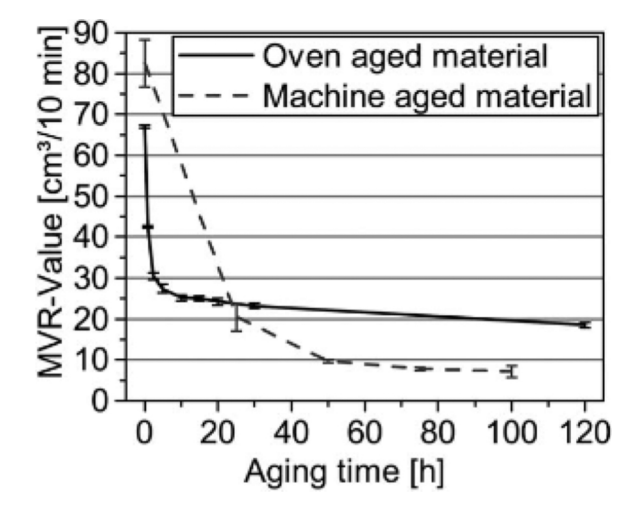


**Fig. 11.** MVR values of EOS PA12 powders oven aged and machine aged [24]. (with permission from publisher).

**Table 5**Aging effects on material rheological property.

| Aging effec   | ets                               | Rheological testing  Viscosity MVR/MFI Melt-state polycondensation, increased chain length[18,70] |                             |
|---------------|-----------------------------------|---|-----------------------------|
| Mechanisn     | 1                                 |   |                             |
| PA12<br>grade | EOS PA12                          | Increase with aging[13, 19,86]  | Decrease with aging [21,24] |
|               | Duraform PA12                     | Increase with aging[87]   | Decrease with aging [16]    |
|               | Orgasol PA12<br>VESTOSINT<br>PA12 | Unchanged[86] Increase and then decrease[18]  | -                           |

The powder bed should be pre-heated to a suitable temperature to ensure good absorption characteristics of powder feedstock and appropriate sintering behavior. During sintering, the pre-heating temperature is kept just below the melting temperature. This practice ensures part-free strains (i.e., crystallization-induced shrinkage and thermal-induced shrinkage) [93,94] are minimized while subsequent layers are melted, leading to a low level of residual stress between layers. A final slow cooling provides a uniform free strain evolution and part dimensional stability.

High melting enthalpy of material is also essential to ensure appropriate sintering behavior through preventing the unused powder from melting on the part surface. Further, appropriate sintering demands that enough molten material with sufficient viscosity spreads to form necks between adjacent particles, forming an increased dense structure with low porosity and better dimensional accuracy.

Though influenced by various process parameters [95–97], the dimensional accuracy of parts printed using aged PA12 powders decreases compared to the original part using the same parameters [18]. Due to aging, particle shape and surface morphology of aged PA12 powders show obvious differences caused by powder aggregation, expansion, and shrinkage. As a result, the absorption characteristics and uniformity of solidification for aged powders both reduce. Consequently, the sintered part using aged powders, in general, has decreased dimensional accuracy of around 5%-10% [18] (Fig. 12).

# 5.1.2. Surface roughness

Due to degradation caused particle aggregation and particle sphericity change, sintering with reclaimed PA12 powders generates part surfaces with severe roughness. Previous studies have shown the "orange peel" phenomenon – an undesirable surface effect (Fig. 13) that occurs commonly when using aged powders [21,78,98,99]. Methods to reduce the surface roughness and eliminate "orange peel" include controlling the SLS process parameters, for instance, energy density and laser scanning strategy [90]. To fabricate parts with good surface quality using aged PA12 powders, Gornet et al. [98] utilized a constant refresh rate with new powders of a high percentage.

# 5.2. Thermo-chemical property changes of the printed part

# 5.2.1. DSC test

We printed parts respectively using the EOS pure new and pure aged PA12 powders (aged at 171  $^{\circ}\text{C}$  after one full printing cycle). The aged powders were sieved before sintering. The printing parameters are: preheating temperature: 160  $^{\circ}\text{C}$ , laser power: 18 W, scan speed: 3000 mm/s, scan spacing: 0.3 mm, layer thickness: 150  $\mu m$ . To gain further understanding of the thermo-chemical properties of printed parts, we conducted DSC tests to these parts.

The DSC curves of the sintered parts exhibit obvious differences from that of the powders in the primary heating cycle (the first heating cycle). The former contains two melting peaks, while one in the latter [44]. For the parts, the first peak results from the melting process of the spherulite chains, while the second peak originates from the melting of core

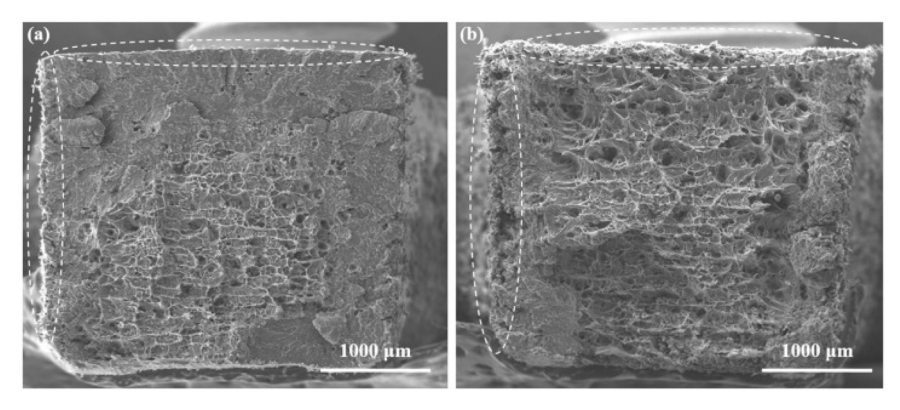


Fig. 12. Cross-section of SLS printed parts using (a) new powders, and (b) 3-time reused powders [18]. (with permission from publisher).

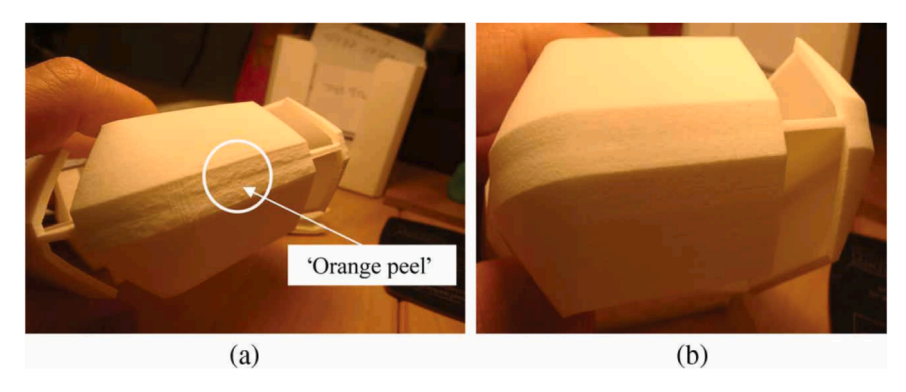


Fig. 13. SLS printed parts (a) with "Orange peel" using aged powders and (b) with good surface finish using new powders [21]. (with permission from publisher).

regions of the aggregated spherulite structures. These spherulites cannot melt during the sintering process and need an elevated temperature to fully melt [18.19].

Moreover, the DSC curves of the sintered part using aged PA12 powders also show differences compared to part using new powders [44]. The DSC curves suggest that aging (i) delays the onset crystallization temperature (aged: 149.70 °C; new: 154.22 °C), and (ii) decreases the peak crystallization temperature (aged: 144.86 °C; new: 148.29 °C) and the crystallization enthalpy (aged: 51.25 J/g; new: 53.67 J/g) of parts using aged powders, resulting from post-condensation [19]. Given that the aged powder has longer molecular chains due to polycondensation, chain mobility is lower in the molten aged powder than molten virgin powder. As a result, a lower crystallinity achieves for part fabricated with aged powder. This reduction is confirmed by a reduction in melting enthalpy (aged: 48.16 J/g; new: 64.51 J/g) observed in DSC tests.

# 5.2.2. Comparisons

Table 6 compares thermo-chemical property changes between parts printed using new and aged (a) EOS GmbH PA12, (b)VESTOSINT X1556 Evonik PA12, and (c) Sinterit PA12 gray. As shown, the onset crystallization temperature, peak crystallization temperature, and crystallization enthalpy of samples using aged powders all decrease in Table 6(a), (b) and (c). The peak melting temperature and melting enthalpy in Table 6(a) decrease after aging, and increase in Table 6(c). In addition to aging/reuse, powder grades also affect the part thermo-chemical property.

# 5.3. Crystalline structure

# 5.3.1. Microstructure

From SEM [19] or optical microscopy [100], the cross-sectional micrograph of a sintered part is divided into four regions. From top to bottom, they are respectively unmolten particle fused to the edge, spherulites from fully melted & crystallized particles, unmolten particle cores, and spherulites from the melted & crystallized region (Fig. 14) [100]. The microstructure of parts can be simply described as the unmolten particle cores surrounded with spherulites [101]. The cores are the unmolten central regions of the sintered powders coming out when these powders do not get enough energy and heat to fully melt. Besides, the cores are believed to be crucial to part post-crystallization and spherulite growth [100].

# 5.3.2. Post-crystallization and spherulite growth

When going through the sintering process, new and aged powders transfer from their solid states to the molten phase. Dissimilar to new powders, aged powders have numerous high-melting-point pieces in their molten phase. These pieces work as nucleation sites to form the nucleation seeds. As a result, the new powders only have a few nucleation seeds due to their fewer high-melting-pieces. However, a large number of nucleation seeds form in the aged ones. The generated nucleation seeds then serve as the basement for spherulite growth during the cooling process when the temperature is below the material melting temperature. After layers of material solidification, lots of spherulites grow on the amorphous solid region of part using aged powders and cannot spread smoothly in the limited space, leading to the formation of coarse spherulites. On the other hand, the spherulites are fibrillar smooth when using new powders. Consequently, due to the aging-induced post-crystallization/spherulite growth,

**Table 6**Thermo-chemical property changes between parts printed using new and aged PA12 powders of different grades.

| PA12 grade                          | PA12, EOS GmbH        |                        |
|-------------------------------------|-----------------------|------------------------|
|                                     | Part using new powder | Part using aged powder |
| Onset melting temperature           | 173.15 °C             | 171.75 °C              |
| Peak melting temperature            | 179.61 °C             | 177.95 °C              |
| Melting enthalpy                    | 64.51 J/g             | 48.16 J/g              |
| Onset crystallization temperature   | 154.22 °C             | 149.70 °C              |
| Peak crystallization<br>temperature | 148.29 °C             | 144.86 °C              |
| Crystallization enthalpy            | 53.67 J/g             | 51.25 J/g              |

| PA12 grade                        | VESTOSINT X1556, Evonik |                                 |  |
|-----------------------------------|-------------------------|---------------------------------|--|
|                                   | Part using new powder   | Part using 3-time reused powder |  |
| Peak melting temperature          | 177.02 °C               | 176.07 °C                       |  |
| Onset crystallization temperature | 150.45 °C               | 149.32 °C                       |  |
| Peak crystallization temperature  | 145.27 °C               | 144.28 °C                       |  |
| Crystallization enthalpy          | 47.65 J/g               | 45.94 J/g                       |  |

| (c) Part using Sinterit PA12 gray[63] |                       |                                 |
|---------------------------------------|-----------------------|---------------------------------|
| PA12 grade                            | Sinterit PA12 gray    |                                 |
|                                       | Part using new powder | Part using 5-time reused powder |
| Onset melting temperature             | 176.37 °C             | 172.54 °C                       |
| Peak melting temperature              | 178.11 °C             | 181.19 °C                       |
| Melting enthalpy                      | 44.30 J/g             | 50.57 J/g                       |
| Onset crystallization temperature     | 154.26 °C             | 153.80 °C                       |
| Peak crystallization temperature      | 151.90 °C             | 151.15 °C                       |
| Crystallization enthalpy              | 51.37 J/g             | 47.52 J/g                       |

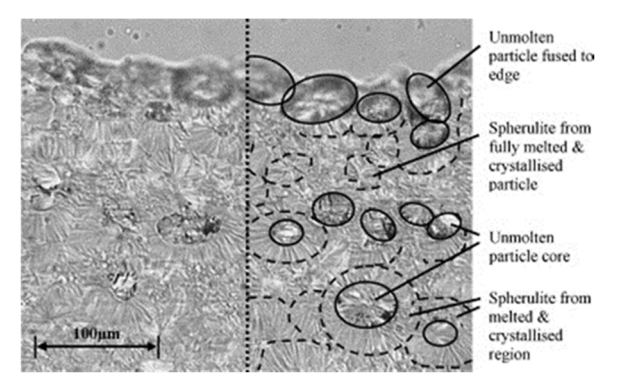


**Fig. 14.** The cross-sectional micrograph of a sintered part [100]. (with permission from publisher).

microstructure of the printed part using aged PA12 powders changes from fibrillar spherulites to coarse spherulites (Fig. 15) [19]. Other work reported the same phenomenon and verified the spherulite growth/coarse spherulites in part using aged PA12 [44,54].

# 5.3.3. Crystalline structure evolution

X-Ray Diffraction (XRD) or Wide-angle X-ray Scattering (WAXS) spectra are commonly used to detect crystalline structure evolution of PA12. Results provide information on the crystallizing procedures and/or crystal transformations between parts from virgin powders and parts from used powders [18,19]. Generally, PA12 presents two crystal

structures: the  $\gamma$ -phase is stable with parallel chain orientation and twisted helical conformations, while the  $\alpha$ -phase is unstable with antiparallel chain orientation [18,86,102,103]. The major difference in XRD results between powder and part is that part exhibits only  $\gamma$  peaks while the powders show mainly  $\alpha$  peaks [18]. Under atmospheric pressure, slow crystallization of the 3D-printed part allows the crystalline chains to transform and form a more stable  $\gamma$  form. However, crystal structure stability for parts from virgin powders and parts from used powders exhibit differences. XRD results show that the intensity of preferable  $\gamma$  reflection reduces with aging, attributed to the decreased chain mobility caused by increased molecular weight and viscosity after aging. Therefore, it is more difficult to form a perfect  $\gamma$  crystal structure for the part from used powders than part from virgin powders.

Fig. 16 shows the WAXS spectra of EOS PA12 powders and the corresponding parts, along with the crystallinity of powders and the corresponding parts [19].  $\gamma$  structure dominates in the parts from used powders (Fig. 16a). Aged powders have a higher crystallinity than new powders (aged: 51%; new: 46%). Due to a reduction in chain mobility caused by polycondensation [18], crystalline ratio of parts from used powders decreases (Fig. 16b) [19,104]. The crystalline ratio affects surface finish (e.g., roughness) and mechanical properties of the 3D printed specimens. Higher crystalline ratios generally result in increases in tensile strengths and Young's modulus, and decreased elongations at break [105].

# 5.4. Density

Density of SLS PA12 components is a critical factor largely influencing fatigue, ductility and strength, etc [24]. Semicrystalline polymers with high molecular weight and long chemical chains have increased entanglements and bonding, decreased chain ends, and free volume, making it easy to achieve a high density [34]. The long chemical chains, increased entanglements and bonding, and increased crystallinity further tend to lower MVR and increase the viscosity of the polymer, resulting in a significant impact on increasing part density. The degree of branching is another factor that can influence polymer density through changing molecular weight [54]. Besides, the environmental temperature and testing conditions also affect part density. Given that voids act as stress risers to reduce strength, density can be directly correlated to mechanical performance.

In Fig. 17, the decreased MVR indicates the EOS GmbH PA12 aging (aged on a DTM Sinterstation 2500HS SLS 3D printer at 174 °C for 120 h) with an origin MVR of 82.5 cm<sup>3</sup>/[10 min]. The aged PA12 materials were processed into parts using an EOS Formiga P100 SLS machine (pre-heating temperature 174 °C, layer thickness 0.1 mm). F1-F4 mean the increased energy density levels (F1: 0.16 J/mm<sup>3</sup>; F2: 0.2 J/ mm<sup>3</sup>; F3: 0.27 J/mm<sup>3</sup>; F4: 0.33 J/mm<sup>3</sup>) [24]. With energy density F1, part density decreases from 0.94 to 0.77 g/cm<sup>3</sup> with material aging (MVR decreasing from 82.5 to 7.1 cm<sup>3</sup>/min). Longer aging time also leads to lower part density [24]. Stored at 140 °C, the density of part using EOS PA12 decreases from 1.00 to 0.98 g/cm<sup>3</sup> after 336 h [54]. Besides, recycling time affects part density. A part using new Sinterit PA12 powder is 0.98 g/cm<sup>3</sup>, while that using 2-time, 5-time and 8-time reused powders are, respectively, 0.92, 0.83, 0.81 g/cm<sup>3</sup> [63]. Density of parts using aged powders decreases compared to that of parts using new powders.

## 5.5. Mechanical properties

Tensile strength [24,28,98,100,106], Young's modulus [24,100], and elongation at break [24,28,98,106] are important for functional applications printed in SLS. The knowledge and theory on mechanical properties of parts using new powders have been studied intensively and show good consistency. However, lots of debates remain on the effects of powder reuse to part mechanical properties. Several reports claimed no significant changes exist in tensile strengths, Young's modulus and

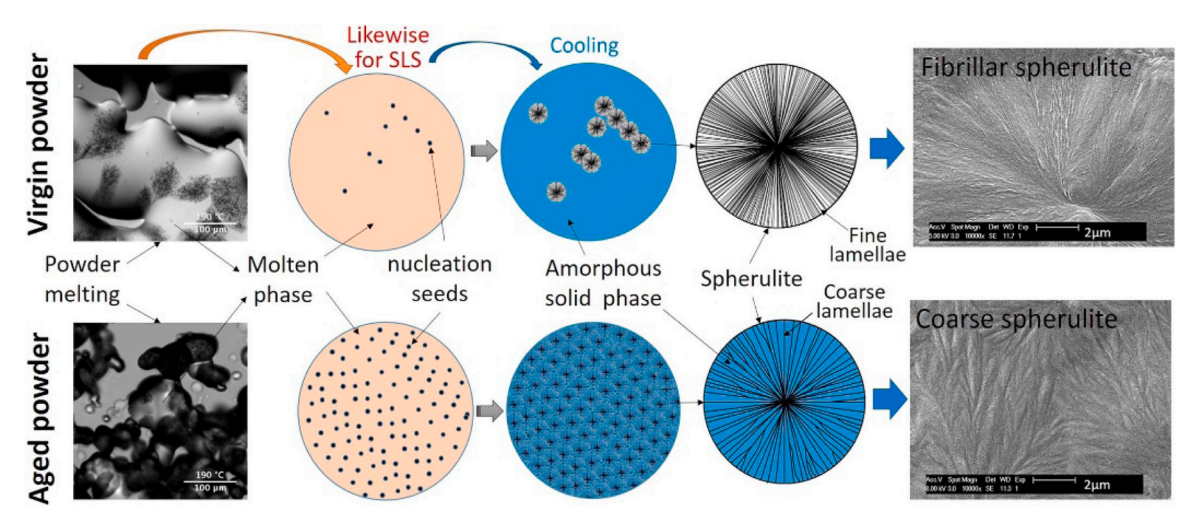


**Fig. 15.** The comparison of microstructures between part using new powders and part using aged powders [19]. (with permission from publisher).

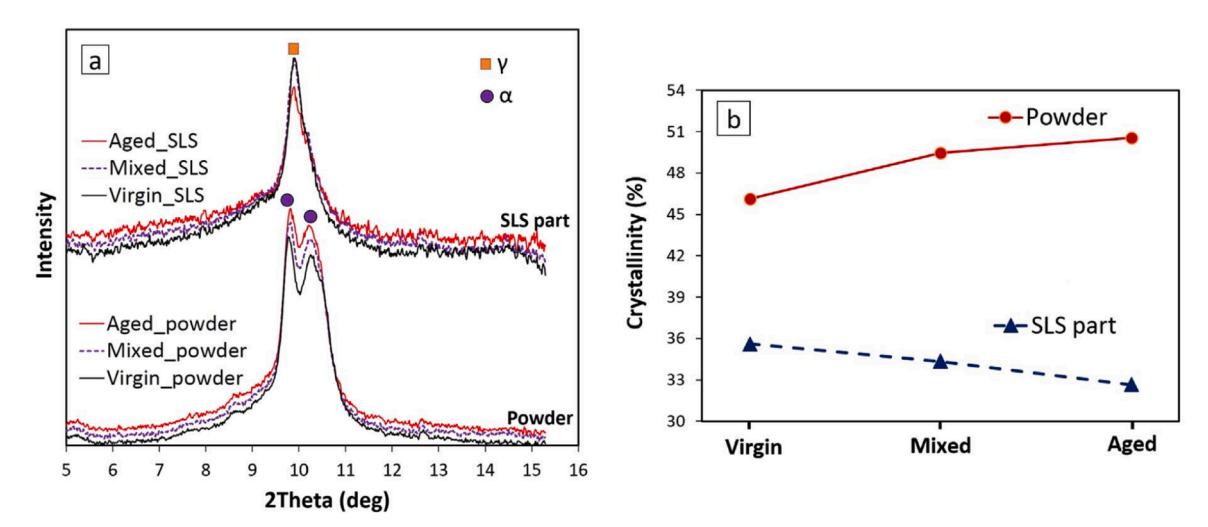
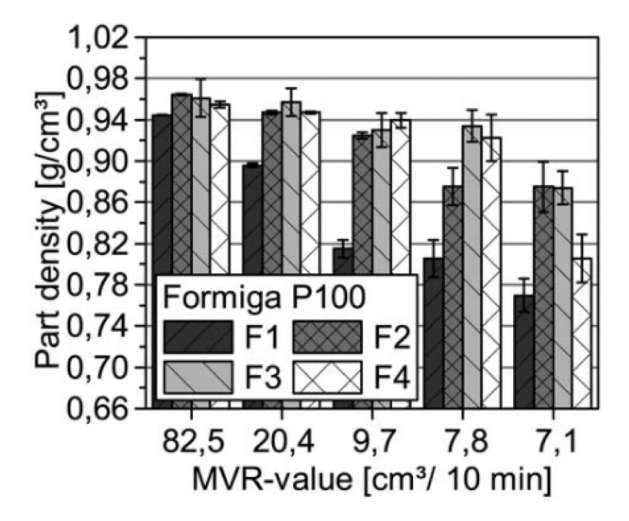


Fig. 16. (a) WAXS spectra for powders and the corresponding parts; (b) Crystallinity of powders and the corresponding parts [19]. (with permission from publisher).



**Fig. 17.** Part density with different aging status [24]. (with permission from publisher).

elongations at break increase for parts using aged powders (Fig. 18) [98, 100,107]. On the other hand, other results report a decreased tensile strength (Table 7a: from 35 N/mm² to 2 N/mm², and Table 7c: from 31.65 Mpa to 20.45 Mpa), a decreased Young's modulus (Table 7b: from 2000 Mpa to 300 Mpa, and Table 7c: from 1275.67 Mpa to 1034.5 Mpa), with a decreased elongation at break (Table 7a: from 5.3% to 0.2%, and Table 7c: from 6.24% to 4.55%) [28,63,106], or with an increased elongation at break (Table 7b, from 9% to 46%) [24,27]. The differences in these studies result from various PA12 powder grades, SLS machine, processing and printing conditions, such as process parameters, test instruments, or humidity conditions. Also, the appropriate selection of process parameters improves the part mechanical properties while multiple-time reuse [29].

When fabricating tensile bars using different PA12 powders and different SLS machines, different sets of processing parameters are applied (Table 7). However, when processing the same kind of PA12 using different SLS equipment, the different sets of processing parameters are also necessary. When sintering EOS GmbH PA12 to produce parts using the Sinterstation 200 SLS 3D printer, the parameters are preheating temperature 175 °C, laser power 5 W, layer thickness 0.1 mm, and scanning speed 1257 mm/s [28]. When sintering EOS GmbH PA12 using the in-house built and customized SLS testbed, the

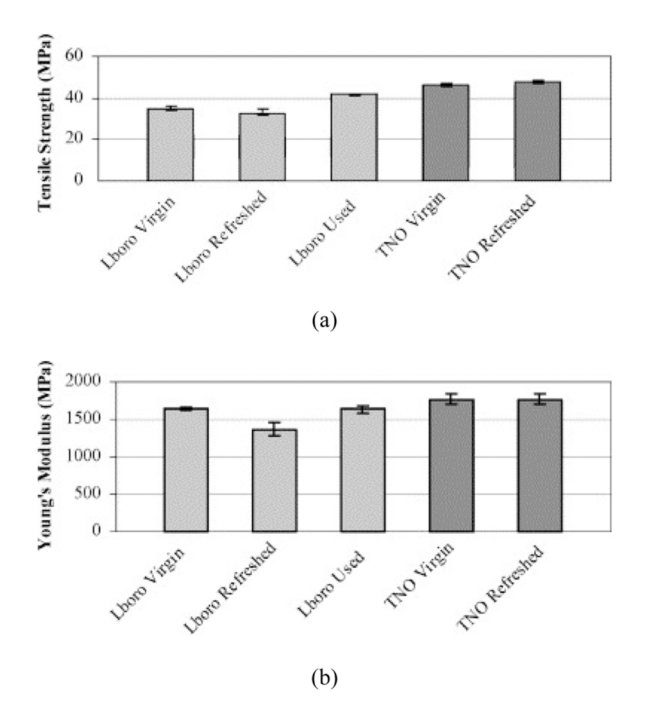


**Fig. 18.** (a) Tensile strength and (b) Young's Modulus remain little changes with reuse [100]. (with permission from publisher).

parameters are preheating temperature 160  $^{\circ}$ C, laser power 18 W, layer thickness 0.15 mm, and scan speed 3000 mm/s [43].

For semicrystalline polymers, the molecular weight, cross-linking, and crystallinity are the main microstructural factors affecting tensile strength of thermoplastics [108–110]. For PA12, a low molecular weight leads to low tensile strength, where the microstructural carbon layers and chains are weakly connected and can move easily. When the molecular weight increases to a large extent, the carbon layers and chains become complex, crosslinked, and bonded by strong van der Waals forces, resulting in the high tensile strength [111]. Similarly, the occurrence of chain cross-linking strengthens the microstructural bonding and connection between layers and chains, restricting the chain motions and improving PA12 tensile strength, while chain scission adversely lowers the tensile strength. Furthermore, high crystallinity or large crystalline area raises PA12 tensile strength through the significantly strengthened intermolecular bonding [109]. In addition, product fabricating orientation, testing velocity and temperature also influence polymer tensile strength.

Different from tensile strength, Young's modulus of semicrystalline polymer is not directly affected by molecular weight [112]. Increasing crystallinity during material degradation raises material Young's modulus. As crystallinity increases, the adjacent aligned chain segments strengthen the interchain bonding, which inhibits relative interchain motion as well [113]. Besides, drawing deformation and annealing also help to increase Young's modulus, by producing the oriented molecular structures and enhanced interchain bonding.

A high elongation at break indicates that the semicrystalline polymer has good ductility, which depends largely on the material's chemical composition. Polymer crystallization largely affects elongation at break. The big crystal size means low ductility that the material is brittle and easy to fracture before deforming much under a tensile load, decreasing polymer elongation at break [43]. Materials with a small crystal size are more likely to deform without breaking, leading to a high elongation at break. Though a high crystalline ratio generally increases tensile strengths and Young's modulus, it decreases elongation at break due to the large crystal sizes and reduced flexibility [105]. Mechanical testing velocity, orientation level, and temperature also affect elongation at

**Table 7**Mechanical properties of part using different PA12 powders with aging/reuse.

| (a) PA12, EOS Gmb   | bH[28]  |   |  |  |
|---------------------|---|---|--|--|
| Printing parameters | • •   | Preheating temperature: 175 °C            |  |  |
|                     |   | Layer thickness: 0.1 mm                   |  |  |
|                     | (Type A)<br>Laser power: 5 W  | Scanning speed:                           |  |  |
|                     | *   | 1257 mm/s                                 |  |  |
| Tensile strength    | 35 N/mm <sup>2</sup> – part using new powder  |   |  |  |
| rensne strength     | 5 N/mm <sup>2</sup> – part using fiew powders   |   |  |  |
|                     | 2 N/mm <sup>2</sup> – part using 10-time reuse  |   |  |  |
| Fracture strain     | 5.3% – part using new powders   | •   |  |  |
|                     | 0.8% – part using 5-time reused pov   |   |  |  |
|                     | 0.2% – part using 10-time reused po   | owder                                     |  |  |
| (b) Duraform PA12   | [27]  |   |  |  |
| Printing parameter  | s Equipment: 3D System  | ns Layer Thickness:                       |  |  |
|                     | Sinterstation   | 0.1 mm                                    |  |  |
|                     | Tensile bar: ISO stand  |   |  |  |
|                     | 527–2, 1996 1 A   | 11 W                                      |  |  |
| Test parameters     | Humidity: 50% RH<br>Machine: Zwick 103 te   | esting machine with a 10 KN               |  |  |
|                     | load cell   | sting indennie with a 10 kg               |  |  |
|                     | Test speed: 5 mm/min  | 1   |  |  |
| Storage 4 Ter       | nsile 43 MPa, storage at 20   | 43 MPa, storage at 20 °C                  |  |  |
| weeks stre          | ength 15 MPa, storage at 14   | 15 MPa, storage at 140 $^{\circ}\text{C}$ |  |  |
|                     |   | 2000 MPa, storage at 20 °C                |  |  |
|                     | dulus 300 MPa, storage at 1   |   |  |  |
| E10<br>bre          | ngation at $9\%$ , storage at $20 ^{\circ}$ C ak $46\%$ , storage at $140 ^{\circ}$ C | C.  |  |  |
| (c) Sinterit PA12[6 | ,   |   |  |  |
|                     |   | v mt·1                                    |  |  |
| Printing            | Equipment: Sharebot SnowWhite   | Layer Thickness:<br>0.1 mm                |  |  |
| parameters          | SLS printer Tensile bar: ASTM standard Type 5   | Laser power: 25% of                       |  |  |
|                     | Tensile bar. ASTWI standard Type 3  | 14 W                                      |  |  |
|                     | Pre-heating time: 600 s   | Plate temperature:                        |  |  |
|                     |   | 160 °C                                    |  |  |
| Test parameters     | At ambient laboratory condition   |   |  |  |
|                     | Machine: MTS Alliance RT/10 test f  | rame, 1000 N load cell                    |  |  |
|                     | Test speed: 10.0 mm/min   |   |  |  |
| Tensile strength    | Part using new powders  | 31.65 Mpa                                 |  |  |
|                     | Part using 2-time reused powders  | 27.17 Mpa                                 |  |  |
|                     | Part using 5-time reused powders  | 21.91 Mpa                                 |  |  |
| Young's modulus     | Part using 8-time reused powders Part using new powders                               | 20.45 Mpa<br>1275.67 Mpa                  |  |  |
| roung s modulus     | Part using 1-time reused powders  | 1275.07 Mpa<br>1190 Mpa                   |  |  |
|                     | Part using 5-time reused powders  | 984.5 Mpa                                 |  |  |
|                     | Part using 8-time reused powders  | 1034.5 Mpa                                |  |  |
| Elongation at       | Part using new powders  | 6.24%                                     |  |  |
| break               | Part using 2-time reused powders  | 5.52%                                     |  |  |
|                     | Part using 5-time reused powders Part using 8-time reused powders                     | 4.89%                                     |  |  |
|                     |   | 4.55%                                     |  |  |

break. Slow testing velocities, small orientations, and increased temperatures allow for higher elongation at break.

# 6. The parameter setting in SLS using aged PA12 powders

After investigating the powder and part property changes, this section provides the parameter setting principles in SLS when using aged PA12 powders. Specifically, we focus on parameters most relevant to process feasibility and material reuse, including pre-heating temperature, energy density, laser power, laser speed, hatch space, and layer thickness [41,105].

# 6.1. Pre-heating temperature

Before sintering polymeric materials with laser beams, thermal radiation pre-heats the powders and raises the temperature of the powder bed chamber to reduce power density requirement during SLS [114].

The principles of setting the pre-heating temperatures for new and aged PA12 powders are similar: both should be near or below the onset melting temperature [18,24,115]. PA12 powders from different suppliers differ slightly in the onset melting temperature. In a DTM 2500plus HiQ SLS printer, Duraform PA12 (onset melting temperature is 180.8 °C) was preheated at 175 °C; Orgasol-IS PA12 (onset melting temperature is 173.6 °C) was preheated at 164 °C [115]. Even using the same grade of PA12 powders, different SLS vendors tune the pre-heating temperature differently, primarily due to the different mechatronics of the machines. For EOS PA12 with melting temperature of 184 °C, the pre-heating temperature was 181°C for the Sinterstation SLS printer and 174 °C for the Formiga SLS printer [24].

# 6.2. Energy density

Energy density is usually defined as the area energy density (Eq. 7) [41,90,116] and the volume energy density (Eq. 8) [31,41].

$$E_{A}(J/mm^{2}) = \frac{LP}{LS \bullet SS}$$
 (7)

$$E_{V}(J/mm^{3}) = \frac{LP}{LS \bullet SS \bullet LT}$$
(8)

Here,  $E_A$  is the area energy density, and  $E_V$  is the volume energy density. LP is laser power, W. LS is laser speed, mm/s. SS is scan spacing, mm. LT is layer thickness, mm.

An appropriate energy density is crucial in the SLS process to guarantee the process feasibility and part quality [117]. Too low or too high energy densities will negatively affect part properties through powder interactions, such as powder bonding, fusion, and degradation. Table 8 lists such corresponding impacts. Specifically, an energy density that is too low leads to weak particle bonding, fusion, and decreased powder thermal degradation due to insufficient thermal motivation and heat effects. On the contrary, a high energy density results in strong bonding and fusion of particles, but more severe thermal degradations in the meantime. Moreover, energy density also greatly affects part properties, for instance, part porosity, density, surface roughness, and mechanical properties (Table 8).

In general, higher energy density leads to better part density and mechanical properties [41]. Identifying the relationships between part properties and energy density is helpful to improve part quality. Even using different energy densities, the properties of parts using new powders are always better than those using mixed or aged powders. Similarly, the properties of parts using one-time recycled powders are better than those using two times recycled powders [41]. The quality of parts using mixed powders and recycled powders can be improved with a higher energy density [53].

Fig. 19 presents that higher energy densities improve the tensile strength of parts 3D-printed using aged powders [24]. F1, F2, F3, and F4 indicate different energy densities of 0.16, 0.20, 0.27 and 0.33 J/mm<sup>3</sup>. With any MVR, part tensile strength with high energy density is larger. It is also worth mentioning that Young's modulus and elongations at break of parts printed with aged powders can also be improved by using higher

**Table 8**The impacts of the low energy density and the high energy density on powder and part properties.

| Items   |                     | Low energy density | High energy density |
|---------|---------------------|--------------------|---------------------|
| Powders | bonding             | weak               | strong              |
|         | fusion              | poor               | good                |
|         | degradation         | low                | high                |
| Parts   | porosity            | more               | less                |
|         | density             | low                | high                |
|         | roughness           | rough              | smooth              |
|         | shrinkage           | low                | high                |
|         | mechanical property | poor               | good                |

energy density, as well as a reduced appearance of "orange peel" on part surface. The improvement is mainly caused by better coalescence resulting from high temperatures and high energy [24]. However, it has limitations for the ranges of energy density used in SLS while processing PA12. Previous studies show that the minimum volume energy density of 0.091 J/mm³ is required to fuse the powder [118,119], indicating very poor connections between the powders and layers. And the maximum energy density recommended in SLS is 0.48 J/mm³ when polymer degradation accelerates [119].

# 6.3. Laser power, laser speed, and hatch space

Laser power has significant effects on mechanical properties and dimensional precision of the 3D-printed part in SLS [120]. As the laser power increases, the increased heat-affected zone leads to the growth of width error. Increasing laser power can improve mechanical properties to a certain extent, but higher powers degrade the powders chemically [107]. This negatively affects the durability and long-term performance of the part, and the recommended range is 10–49.5 W. Laser speed (4000 mm/s-11,500 mm/s) is related closely to part porosity and part flexural modulus [24,31,115,117]. However, sensitivity analysis suggests that laser speed has fewer influences than laser power on the density and mechanical property of the final manufactured specimens [116]. The hatch space (0.1–0.3 mm) affects energy density (larger hatch space decreases energy density), and is together with the layer thickness both impacting significantly the part density and mechanical property when the remaining parameters are constants [31].

### 6.4. Layer thickness

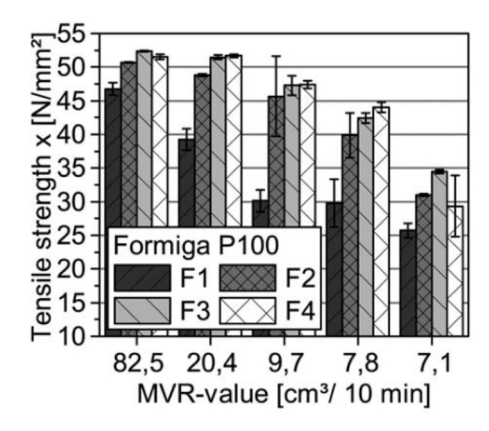
For polymer SLS, parts are usually fabricated with layer thicknesses from 0.06 mm to 0.18 mm in a layer-by-layer manufacturing style for either new powder or aged powder [24,31]. Parts with a smaller layer thickness normally have better mechanical properties, due to the better compaction and uniformity between layers when the layer thickness is small. Table 9 exhibits the recommended process parameter sets for PA12 powder in SLS processing.

# 7. Conclusions

SLS is the most rapidly growing additive manufacturing method suitable for a wide range of materials, given that high-quality complex parts can be fabricated using this method. This review elaborates important research status of aging behaviors and reusability of PA12 powders, and the impact on the performance of printed parts. Starting with the aging mechanisms at the molecular scale, we discussed how material aging rises from the thermal oxidation reactions accompanied by chain crosslinking, chain scission, and post-condensation. Studies exhibit that surface morphology, microstructures, thermo-chemical properties, and flowability of the aged powders vary compared with the new powders, while the size distribution remaining nearly unchanged.

Properties of parts using aged PA12 powders also show differences compared with parts from new powders. The microstructures of parts using aged powders present coarse spherulites and degraded surface morphology, yielding rougher surface smoothness. Parameter controls have been proposed to remedy the problem. For thermo-chemical properties of parts using aged powders, the onset melting temperature decreases, the melting shoulder intervals widen, and the crystallization enthalpy decreases. These changes originate from the thermal breakdown of crystalline spherulites, the reduction of high-melting-point particles, and post-condensation. The mechanical properties of parts 3D-printed with aged PA12 depend largely on powder grades, the status of powder degradation, and process controls. Literature results differ in the control of part properties with reclaimed and reused powders.

Finally, we review how key process parameters impact SLS with aged



# (a) Part tensile strength in the x-direction

# 

80

# (b)Part tensile strength in the z-direction

**Fig. 19.** Part properties as a function of MVR values when using EOS Formiga P100 [24]. (with permission from publisher).

 Table 9

 Recommended process parameter sets for PA12 powder [31,41,117].

| Item                    | Recommended Value                               |
|-------------------------|---|
| Pre-heating temperature | Near the melting point                          |
| Energy density          | $0.091 \text{ J/mm}^3 \sim 0.48 \text{ J/mm}^3$ |
| Laser power             | 10 W ~ 49.5 W                                   |
| Laser speed             | 4000 mm/s ~ 11,500 mm/s                         |
| Hatch space             | $0.1 \text{ mm} \sim 0.3 \text{ mm}$            |
| Layer thickness         | $0.06~mm\sim0.18~mm$                            |

powder materials. Included signature parameters are pre-heating temperature, energy density, laser power, laser speed, hatch space, and layer thickness. Higher energy density can improve the mechanical property of the 3D-printed parts.

# CRediT authorship contribution statement

**Feifei Yang:** Conceptualization, Investigation, Writing – original draft, Writing – review & editing; **Navid Zobeiry:** Visualization, Writing – review & editing; **Ramulu Mamidala:** Visualization, Writing – review & editing; **Xu Chen:** Conceptualization, Methodology, Writing – review & editing.

# **Declaration of Competing Interest**

The authors declare that they have no known competing financial interests or personal relationships that could have appeared to influence the work reported in this paper.

# Acknowledgements

The authors gratefully appreciate Professor David Bourell for providing inputs in previewing the paper and the financial support from Unilever. This material is based upon work supported in part by the National Science Foundation under Grant No. 1953155. Any opinions expressed herein are those of the authors and do not represent those of the sponsors.

# References

- [1] W. Gao, Y. Zhang, D. Ramanujan, K. Ramani, Y. Chen, C.B. Williams, C.C. Wang, Y.C. Shin, S. Zhang, P.D. Zavattieri, The status, challenges, and future of additive manufacturing in engineering, Comput. Aided Des. 69 (2015) 65–89.
- [2] H. Tiismus, A. Kallaste, T. Vaimann, A. Rassölkin, A. Belahcen, Additive Manufacturing of Prototype Axial Flux Switched Reluctance Electrical Machine,

in: 2021 28th International Workshop on Electric Drives: Improving Reliability of Electric Drives (IWED), IEEE, 2021, pp. 1–4.

Formiga P100

- [3] R. Jemghili, A.A. Taleb, K. Mansouri, Additive Manufacturing Progress as a New Industrial Revolution, in: 2020 IEEE 2nd International Conference on Electronics, Control, Optimization and Computer Science (ICECOCS), IEEE, 2020, pp. 1–8.
- [4] M. Schmid, A. Amado, K. Wegener, Materials perspective of polymers for additive manufacturing with selective laser sintering, J. Mater. Res. 29 (2014) 1824–1832.
- [5] C. Zhou, Y. Chen, Additive manufacturing based on optimized mask video projection for improved accuracy and resolution, J. Manuf. Process. 14 (2012) 107–118.
- [6] A.-N. Chen, J.-M. Wu, K. Liu, J.-Y. Chen, H. Xiao, P. Chen, C.-H. Li, Y.-S. Shi, High-performance ceramic parts with complex shape prepared by selective laser sintering: a review, Adv. Appl. Ceram. 117 (2018) 100–117.
- [7] S. Müller, P. Woizeschke, Feasibility of a laser powder bed fusion process for additive manufacturing of hybrid structures using aluminum-titanium powdersubstrate pairings, Addit. Manuf. 48 (2021), 102377.
- [8] S. Impey, P. Saxena, K. Salonitis, Selective laser sintering induced residual stresses: precision measurement and prediction, J. Manuf. Mater. Process. 5 (2021) 101.
- [9] K. Hariharan, G. Arumaikkannu, T. Ramkumar, M. Selvakumar, Material stability investigation of polyamide material before and after laser sintering, Int. J. Polym. Anal. Charact. 25 (2020) 158–165.
- [10] A. Awad, F. Fina, A. Goyanes, S. Gaisford, A.W. Basit, 3D printing: principles and pharmaceutical applications of selective laser sintering, Int. J. Pharm. 586 (2020), 119594.
- [11] C. Yan, Y. Shi, L. Hao, Investigation into the differences in the selective laser sintering between amorphous and semi-crystalline polymers, Int. Polym. Process. 26 (2011) 416-423.
- [12] L. Feng, Y. Wang, Q. Wei, PA12 powder recycled from SLS for FDM, Polymers 11 (2019) 727.
- [13] F. Paolucci, M. van Mook, L. Govaert, G. Peters, Influence of post-condensation on the crystallization kinetics of PA12: From virgin to reused powder, Polymer 175 (2019) 161–170
- [14] C. Mielicki, B. Gronhoff, J. Wortberg, Effects of laser sintering processing time and temperature on changes in polyamide 12 powder particle size, shape and distribution, in: AIP Conference Proceedings, American Institute of Physics, 2014, pp. 728–731.
- [15] M. Vasquez, B. Haworth, N. Hopkinson, Methods for quantifying the stable sintering region in laser sintered polyamide-12, Polym. Eng. Sci. 53 (2013) 1230–1240
- [16] M. Uddin, D. Williams, A. Blencowe, Recycling of selective laser sintering waste nylon powders into fused filament fabrication parts reinforced with Mg particles, Polymers 13 (2021) 2046.
- [17] L. Wang, A. Kiziltas, D.F. Mielewski, E.C. Lee, D.J. Gardner, Closed-loop recycling of polyamide12 powder from selective laser sintering into sustainable composites, J. Clean. Prod. 195 (2018) 765–772.
- [18] P. Chen, M. Tang, W. Zhu, L. Yang, S. Wen, C. Yan, Z. Ji, H. Nan, Y. Shi, Systematical mechanism of Polyamide-12 aging and its micro-structural evolution during laser sintering, Polym. Test. 67 (2018) 370–379.
- [19] S. Dadbakhsh, L. Verbelen, O. Verkinderen, D. Strobbe, P. Van Puyvelde, J.-P. Kruth, Effect of PA12 powder reuse on coalescence behaviour and microstructure of SLS parts. Eur. Polym. J. 92 (2017) 250–262.
- [20] K. Dotchev, W. Yusoff, Recycling of polyamide 12 based powders in the laser sintering process, Rapid Prototyp. J. (2009).
- [21] D.T. Pham, K. Dotchev, W. Yusoff, Deterioration of polyamide powder properties in the laser sintering process, Proc. Inst. Mech. Eng. Part C J. Mech. Eng. Sci. 222 (2008) 2163–2176.

- [22] T. Peng, K. Kellens, R. Tang, C. Chen, G. Chen, Sustainability of additive manufacturing: an overview on its energy demand and environmental impact, Addit. Manuf. 21 (2018) 694–704.
- [23] K. Wudy, D. Drummer, Aging effects of polyamide 12 in selective laser sintering: molecular weight distribution and thermal properties, Addit. Manuf. 25 (2019) 1–9
- [24] A. Wegner, C. Mielicki, T. Grimm, B. Gronhoff, G. Witt, J. Wortberg, Determination of robust material qualities and processing conditions for laser sintering of polyamide 12, Polym. Eng. Sci. 54 (2014) 1540–1554.
- [25] S. Josupeit, H.J. Schmid, Experimental analysis and modeling of local ageing effects during laser sintering of polyamide 12 in regard to individual thermal histories, J. Appl. Polym. Sci. 134 (2017) 45435.
- [26] P. Chen, H. Wu, W. Zhu, L. Yang, Z. Li, C. Yan, S. Wen, Y. Shi, Investigation into the processability, recyclability and crystalline structure of selective laser sintered Polyamide 6 in comparison with Polyamide 12, Polym. Test. 69 (2018) 366–374.
- [27] R. Goodridge, R. Hague, C. Tuck, Effect of long-term ageing on the tensile properties of a polyamide 12 laser sintering material, Polym. Test. 29 (2010) 483-493
- [28] K. Wudy, D. Drummer, F. Kühnlein, M. Drexler, Influence of degradation behavior of polyamide 12 powders in laser sintering process on produced parts, in: AIP Conference Proceedings, American Institute of Physics, 2014, pp. 691–695.
- [29] K. Kozlovsky, J. Schiltz, T. Kreider, M. Kumar, S. Schmid, Mechanical properties of reused nylon feedstock for powder-bed additive manufacturing in orthopedics, Procedia Manuf. 26 (2018) 826–833.
- [30] B. Yao, Z. Li, F. Zhu, Effect of powder recycling on anisotropic tensile properties of selective laser sintered PA2200 polyamide, Eur. Polym. J. 141 (2020), 110093.
- [31] A. Wegner, G. Witt, Correlation of process parameters and part properties in laser sintering using response surface modeling, Phys. Procedia 39 (2012) 480–490.
- [32] M. Pavan, M. Faes, D. Strobbe, B. Van Hooreweder, T. Craeghs, D. Moens, W. Dewulf, On the influence of inter-layer time and energy density on selected critical-to-quality properties of PA12 parts produced via laser sintering, Polym. Test. 61 (2017) 386–395.
- [33] B. Caulfield, P.E. McHugh, S. Lohfeld, Dependence of mechanical properties of polyamide components on build parameters in the SLS process, J. Mater. Process. Technol. 182 (2007) 477–488.
- [34] B. Van Hooreweder, F. De Coninck, D. Moens, R. Boonen, P. Sas, Microstructural characterization of SLS-PA12 specimens under dynamic tension/compression excitation, Polym. Test. 29 (2010) 319–326.
- [35] H.C. Kim, H.T. Hahn, Y.S. Yang, Synthesis of PA12/functionalized GNP nanocomposite powders for the selective laser sintering process, J. Compos. Mater. 47 (2013) 501–509.
- [36] R. Paggi, V. Beal, G. Salmoria, Process optimization for PA12/MWCNT nanocomposite manufacturing by selective laser sintering, Int. J. Adv. Manuf. Technol. 66 (2013) 1977–1985.
- [37] C. Balemans, S.F. Looijmans, G. Grosso, M.A. Hulsen, P.D. Anderson, Numerical analysis of the crystallization kinetics in SLS, Addit. Manuf. 33 (2020), 101126.
- [38] P. Peyre, Y. Rouchausse, D. Defauchy, G. Régnier, Experimental and numerical analysis of the selective laser sintering (SLS) of PA12 and PEKK semi-crystalline polymers, J. Mater. Process. Technol. 225 (2015) 326–336.
- [39] D. Soldner, S. Greiner, C. Burkhardt, D. Drummer, P. Steinmann, J. Mergheim, Numerical and experimental investigation of the isothermal assumption in selective laser sintering of PA12, Addit. Manuf. 37 (2021), 101676.
- [40] J. Bai, R.D. Goodridge, R.J. Hague, M. Song, M. Okamoto, Influence of carbon nanotubes on the rheology and dynamic mechanical properties of polyamide-12 for laser sintering, Polym. Test. 36 (2014) 95–100.
- [41] E.C. Hofland, I. Baran, D.A. Wismeijer, Correlation of process parameters with mechanical properties of laser sintered PA12 parts, Adv. Mater. Sci. Eng. (2017) (2017)
- [42] J. Munguia, K. Dalgarno, Fatigue behaviour of laser-sintered PA12 specimens under four-point rotating bending, Rapid Prototyp. J. 20 (2014) 291–300.
- [43] F. Yang, T. Jiang, G. Lalier, J. Bartolone, X. Chen, A process control and interlayer heating approach to reuse polyamide 12 powders and create parts with improved mechanical properties in selective laser sintering, J. Manuf. Process. 57 (2020) 828–846.
- [44] F. Yang, T. Jiang, G. Lalier, J. Bartolone, X. Chen, Process control of surface quality and part microstructure in selective laser sintering involving highly degraded polyamide 12 materials, Polym. Test. 93 (2021), 106920.
- [45] F. Yang, T. Jiang, X. Chen, G. Lalier, J. Bartolone, Active Interlayer Heating for Sustainable Selective Laser Sintering With Reclaimed Polyamide 12 Powders, in: International Symposium on Flexible Automation, American Society of Mechanical Engineers, 2020, pp. V001T009A007.
- [46] Y. Zhuang, Y. Guo, J. Li, K. Jiang, H. Zhang, D. Meng, Study on process and parameter optimisation of selective laser sintering of thermoplastic polyurethane/carbon nanotube powder, Int. J. Adv. Manuf. Technol. 116 (2021) 993–1001.
- [47] C.G. Campbell, D.J. Astorga, E. Martinez, M. Celina, Selective laser sintering (SLS)-printable thermosetting resins via controlled conversion, MRS Commun. (2021) 1–6.
- [48] J.-P. Kruth, X. Wang, T. Laoui, L. Froyen, Lasers and materials in selective laser sintering, Assem. Autom. (2003).
- [49] S. Kumar, A. Czekanski, Roadmap to sustainable plastic additive manufacturing, Mater. Today Commun. 15 (2018) 109–113.
- [50] M. Schmid, A. Amado, K. Wegener, Polymer powders for selective laser sintering (SLS), in: AIP Conference proceedings, AIP Publishing LLC, 2015, pp. 160009.

- [51] Y. Zhou, S. Xi, Y. Huang, M. Kong, Q. Yang, G. Li, Preparation of near-spherical PA12 particles for selective laser sintering via Plateau-Rayleigh instability of molten fibers, Mater. Des. 190 (2020), 108578.
- [52] N. Ma, W. Liu, L. Ma, S. He, H. Liu, Z. Zhang, A. Sun, M. Huang, C. Zhu, Crystal transition and thermal behavior of Nylon 12, e Polym. 20 (2020) 346–352.
- [53] K. Wudy, D. Drummer, Aging behavior of polyamide 12: interrelation between bulk characteristics and part properties, in: Solid Freeform Fabrication Symposium—an Additive Manufacturing Conference, 2016, pp. 770–781.
- [54] A. Wörz, K. Wudy, D. Drummer, A. Wegner, G. Witt, Comparison of long-term properties of laser sintered and injection molded polyamide 12 parts, J. Polym. Eng. 38 (2018) 573–582.
- [55] N. Vidakis, M. Petousis, L. Tzounis, A. Maniadi, E. Velidakis, N. Mountakis, J. D. Kechagias, Sustainable additive manufacturing: mechanical response of polyamide 12 over multiple recycling processes, Materials 14 (2021) 466.
- [56] A.K. Battu, T.R. Pope, T. Varga, J.F. Christ, M.D. Fenn, W.S. Rosenthal, W. Kuang, M. Thomas, A.M. Arnold, M. Schram, Build orientation dependent microstructure in polymer laser sintering: Relationship to part performance and evolution with aging, Addit. Manuf. 36 (2020), 101464.
- [57] D. Drummer, K. Wudy, M. Drexler, Modelling of the aging behavior of polyamide 12 powder during laser melting process, in: AIP Conference Proceedings, AIP Publishing LLC, 2015, pp. 160007.
- [58] R. Li, X. Hu, Study on discoloration mechanism of polyamide 6 during thermooxidative degradation, Polym. Degrad. Stab. 62 (1998) 523–528.
- [59] F. Yang, X. Chen, A combined theoretical and experimental approach to model polyamide 12 degradation in selective laser sintering additive manufacturing, J. Manuf. Process. 70 (2021) 271–289.
- [60] C. Kummert, S. Josupeit, H.-J. Schmid, Thermoplastic elastomer part color as function of temperature histories and oxygen atmosphere during selective laser sintering, JOM 70 (2018) 425–430.
- [61] K. Leja, G. Lewandowicz, Polymer biodegradation and biodegradable polymers-a review, Pol. J. Environ. Stud. 19 (2010).
- [62] Y. Shu, L. Ye, T. Yang, Study on the long-term thermal-oxidative aging behavior of polyamide 6, J. Appl. Polym. Sci. 110 (2008) 945–957.
- [63] F. Yang, A. Schnuerch, X. Chen, Quantitative influences of successive reuse on thermal decomposition, molecular evolution, and elemental composition of polyamide 12 residues in selective laser sintering, Int. J. Adv. Manuf. Technol. (2021) 1–18.
- [64] S. Rhee, J.L. White, Crystal structure and morphology of biaxially oriented polyamide 12 films, J. Polym. Sci. Part B Polym. Phys. 40 (2002) 1189–1200.
- [65] N. Hiramatsu, S. Hashida, S. Hirakawa, Formation of α form Nylon 12 under high pressure, Jpn. J. Appl. Phys. 21 (1982) 651.
- [66] M.A. Czarnecki, P. Wu, H.W. Siesler, 2D FT-NIR and FT-IR correlation analysis of temperature-induced changes of nylon 12, Chem. Phys. Lett. 283 (1998) 326–332.
- [67] C. El-Mazry, M.B. Hassine, O. Correc, X. Colin, Thermal oxidation kinetics of additive free polyamide 6-6, Polym. Degrad. Stab. 98 (2013) 22–36.
- [68] L. Rincon-Rubio, B. Fayolle, L. Audouin, J. Verdu, A general solution of the closed-loop kinetic scheme for the thermal oxidation of polypropylene, Polym. Degrad. Stab. 74 (2001) 177–188.
- [69] F.M. Mwania, M. Maringa, K. van der Walt, A review of methods used to reduce the effects of high temperature associated with polyamide 12 and polypropylene laser sintering, Adv. Polym. Technol. 2020 (2020).
- [70] M.A. Schaffer, K.B. McAuley, M.F. Cunningham, E.K. Marchildon, Experimental study and modeling of nylon polycondensation in the melt phase, Ind. Eng. Chem. Res. 42 (2003) 2946–2959.
- [71] N. Hesse, M.A. Dechet, J.S.G. Bonilla, C. Lübbert, S. Roth, A. Bück, J. Schmidt, W. Peukert, Analysis of tribo-charging during powder spreading in Selective Laser Sintering: assessment of polyamide 12 powder ageing effects on charging behavior, Polymers 11 (2019) 609.
- $\ \ \,$  [72] E. Dijkstra-Vinken, Polyamides: Hydrogen bonding, the Brill transition, and superheated water, 2008.
- [73] R. Dai, M. Huang, L. Ma, W. Liu, S. He, H. Liu, C. Zhu, Y. Wang, Z. Zhang, A. Sun, Study on crystal structure and phase transitions of polyamide 12 via wide-angle X-ray diffraction with variable temperature, Adv. Compos. Hybrid. Mater. 3 (2020) 522–529.
- [74] O. Verkinderen, D. Baeten, P. Van Puyvelde, B. Goderis, The crystallization of PA11, PA12, and their random copolymers at increasing supercooling: From eutectic segregation to mesomorphic solid solutions, Polym. Cryst. 4 (2021), e10216.
- [75] C. Wan, F. Zhao, X. Bao, B. Kandasubramanian, M. Duggan, Effect of POSS on crystalline transitions and physical properties of polyamide 12, J. Polym. Sci. Part B Polym. Phys. 47 (2009) 121–129.
- [76] E.J. Parteli, T. Pöschel, Particle-based simulation of powder application in additive manufacturing, Powder Technol. 288 (2016) 96–102.
- [77] R.J. Young, P.A. Lovell, Introduction to Polymers, CRC Press, 2011.
- [78] W. Yusoff, H. Ani, D. Pham, K. Dotchev, Influence of molecular weight average, degree of crystallinity, and viscosity of different polyamide PA12 powder grades on the microstructures of laser sintered part, in: MATEC Web of Conferences, EDP Sciences, 2015, pp. 03005.
- [79] G. Craft, J. Nussbaum, N. Crane, J. Harmon, Impact of extended sintering times on mechanical properties in PA-12 parts produced by powderbed fusion processes, Addit. Manuf. 22 (2018) 800–806.
- [80] S. Gogolewski, K. Czerntawska, M. Gastorek, Effect of annealing on thermal properties and crystalline structure of polyamides. Nylon 12 (polylaurolactam), Colloid Polym. Sci. 258 (1980) 1130–1136.

- [81] D. Schulze, Powders and Bulk Solids, Behaviour, Characterization, Storage and Flow, Springer, 2008.
- [82] S. Yang, J. Evans, Metering and dispensing of powder; the quest for new solid freeforming techniques, Powder Technol. 178 (2007) 56–72.
- [83] S. Ziegelmeier, F. Wöllecke, C. Tuck, R. Goodridge, R. Hague, Characterizing the bulk & flow behaviour of LS polymer powders, in: Proceedings SFF Symposium, Austin (TX), USA, 2013.
- [84] M. Krantz, H. Zhang, J. Zhu, Characterization of powder flow: static and dynamic testing, Powder Technol. 194 (2009) 239–245.
- [85] S.C. Ligon, R. Liska, Jr Stampfl, M. Gurr, R. Mulhaupt, Polymers for 3D printing and customized additive manufacturing, Chem. Rev. 117 (2017) 10212–10290.
- [86] L. Verbelen, S. Dadbakhsh, M. Van den Eynde, J.-P. Kruth, B. Goderis, P. Van Puyvelde, Characterization of polyamide powders for determination of laser sintering processability, Eur. Polym. J. 75 (2016) 163–174.
- [87] S. Weinmann, C. Bonten, Recycling of PA12 powder for selective laser sintering, in: AIP Conference Proceedings, AIP Publishing LLC, 2020, pp. 020056.
- [88] A. Martínez, A. Ibáñez, A. Sánchez, M. León, Comparison of aged polyamide powders for selective laser sintering, in: AIP Conference Proceedings, American Institute of Physics, 2012, pp. 5–13.
- [89] F.A.C. Sanchez, H. Boudaoud, S. Hoppe, M. Camargo, Polymer recycling in an open-source additive manufacturing context: Mechanical issues, Addit. Manuf. 17 (2017) 87–105.
- [90] W. Yusoff, A. Thomas, The Effect of Employing an Effective Laser Sintering Scanning Strategy and Energy Density Value on Eliminating "Orange Peel" on A Selective Laser Sintered Part, International Association for Management of Technology, 2008.
- [91] R.S. Evans, D.L. Bourell, J.J. Beaman, M.I. Campbell, Rapid manufacturing of silicon carbide composites, Rapid Prototyp. J. (2005).
- [92] Y. Guo, K. Jiang, D.L. Bourell, Accuracy and mechanical property analysis of LPA12 parts fabricated by laser sintering, Polym. Test. 42 (2015) 175–180.
- [93] N. Zobeiry, A. Poursartip, The Origins of Residual Stress and Its Evaluation in Composite Materials, In: Structural Integrity and Durability of Advanced Composites, Elsevier, 2015, pp. 43–72.
- [94] N. Zobeiry, A. Forghani, C. Li, K. Gordnian, R. Thorpe, R. Vaziri, G. Fernlund, A. Poursartip, Multiscale characterization and representation of composite materials during processing, Philos. Trans. R. Soc. A Math. Phys. Eng. Sci. 374 (2016) 20150278.
- [95] R.-J. Wang, L. Wang, L. Zhao, Z. Liu, Influence of process parameters on part shrinkage in SLS, Int. J. Adv. Manuf. Technol. 33 (2007) 498–504.
- [96] G. Strano, L. Hao, R. Everson, K. Evans, Multi-objective optimization of selective laser sintering processes for surface quality and energy saving, Proc. Inst. Mech. Eng. Part B J. Eng. Manuf. 225 (2011) 1673–1682.
- [97] C.C. Seepersad, T. Govett, K. Kim, M. Lundin, D. Pinero, A designer's guide for dimensioning and tolerancing SLS parts, in: 2012 International Solid Freeform Fabrication Symposium, University of Texas at Austin, 2012.
- [98] T. Gornet, K. Davis, T. Starr, K. Mulloy, Characterization of Selective Laser Sintering™ Materials to Determine Process Stability 546, in: 2002 International Solid Freeform Fabrication Symposium, 2002.
- [99] J.-P. Kruth, G. Levy, F. Klocke, T. Childs, Consolidation phenomena in laser and powder-bed based layered manufacturing, CIRP Ann. 56 (2007) 730–759.
- [100] H. Zarringhalam, N. Hopkinson, N. Kamperman, J. De Vlieger, Effects of processing on microstructure and properties of SLS Nylon 12, Mater. Sci. Eng.: A 435 (2006) 172–180
- [101] E. Moeskops, N. Kamperman, B. van de Vorst, R. Knoppers, Creep behaviour of polyamide in selective laser sintering, in: 2004 International Solid Freeform Fabrication Symposium, 2004.

- [102] L. Telen, P. Van Puyvelde, B. Goderis, Random copolymers from polyamide 11 and polyamide 12 by reactive extrusion: synthesis, eutectic phase behavior, and polymorphism, Macromolecules 49 (2016) 876–890.
- [103] C. Cai, W.S. Tey, J. Chen, W. Zhu, X. Liu, T. Liu, L. Zhao, K. Zhou, Comparative study on 3D printing of polyamide 12 by selective laser sintering and multi jet fusion, J. Mater. Process. Technol. 288 (2021), 116882.
- [104] L. Li, M.H. Koch, W.H. de Jeu, Crystalline structure and morphology in nylon-12: a small-and wide-angle X-ray scattering study, Macromolecules 36 (2003) 1626–1632.
- [105] C.C. Kai, Y.W. Yee, T.M. Jen, L.E. Jia, Understanding the link between process parameters, microstructure and mechanical properties of laser sintered PA12 parts through X-ray computed tomography, 2016.
- [106] F. Kuehnlein, D. Drummer, D. Rietzel, A. Seefried, Degradation Behavior and Material Properties of PA 12 Plastic Powders Processed by Powder Based Additive Manufacturing Technologies, na, 2010.
- [107] J. Choren, V. Gervasi, T. Herman, S. Kamara, J. Mitchell, SLS powder life study, in: 2001 International Solid Freeform Fabrication Symposium, 2001.
- [108] A. Touris, A. Turcios, E. Mintz, S.R. Pulugurtha, P. Thor, M. Jolly, U. Jalgaonkar, Effect of molecular weight and hydration on the tensile properties of polyamide 12, Results Mater. 8 (2020), 100149.
- [109] S. Chatterjee, F. Nüesch, B. Chu, Crystalline and tensile properties of carbon nanotube and graphene reinforced polyamide 12 fibers, Chem. Phys. Lett. 557 (2013) 92–96.
- [110] S.-L. Sindinger, C. Kralovec, D. Tasch, M. Schagerl, Thickness dependent anisotropy of mechanical properties and inhomogeneous porosity characteristics in laser-sintered polyamide 12 specimens, Addit. Manuf. 33 (2020), 101141.
- [111] F. Bobaru, Influence of van der Waals forces on increasing the strength and toughness in dynamic fracture of nanofibre networks: a peridynamic approach, Model. Simul. Mater. Sci. Eng. 15 (2007) 397.
- [112] A. Gleadall, Mechanical Properties of Biodegradable Polymers for Medical Applications, In: Modelling Degradation of Bioresorbable Polymeric Medical Devices, Elsevier, 2015, pp. 163–199.
- [113] J. Beauson, G. Schillani, L. Van der Schueren, S. Goutianos, The effect of processing conditions and polymer crystallinity on the mechanical properties of unidirectional self-reinforced PLA composites, Compos. Part A Appl. Sci. Manuf. 152 (2022), 106668.
- [114] X.-f Li, J.-h Dong, Study on curve of Pe-heating temperature control in selective laser sintering, in: Proceedings. The 2009 International Symposium on Web Information Systems and Applications (WISA 2009), Citeseer, 2009, pp. 156.
- [115] M. Schmid, R. Kleijnen, M. Vetterli, K. Wegener, Influence of the origin of polyamide 12 powder on the laser sintering process and laser sintered parts, Appl. Sci. 7 (2017) 462.
- [116] V. Beal, R. Paggi, G. Salmoria, A. Lago, Statistical evaluation of laser energy density effect on mechanical properties of polyamide parts manufactured by selective laser sintering, J. Appl. Polym. Sci. 113 (2009) 2910–2919.
- [117] S. Akande, K. Dalgarno, J. Munguia, J. Pallari, Assessment of tests for use in process and quality control systems for selective laser sintering of polyamide powders, J. Mater. Process. Technol. 229 (2016) 549–561.
- [118] T.L. Starr, T.J. Gornet, J.S. Usher, The effect of process conditions on mechanical properties of laser-sintered nylon, Rapid Prototyp. J. (2011).
- [119] P.K. Jain, P.M. Pandey, P. Rao, Effect of delay time on part strength in selective laser sintering, Int. J. Adv. Manuf. Technol. 43 (2009) 117–126.
- [120] M. Monzón, P.M. Hernández, A.N. Benftez, M.D. Marrero, Á. Fernández, Predictability of plastic parts behaviour made from rapid manufacturing, Tsinghua Sci. Technol. 14 (2009) 100–107.